NEW INSTRUMENTS AND MEASUREMENT METHODS

Mirror electron microscopy

A. E. Luk'yanov, G. V. Spivak, and R. S. Gvozdover

M. V. Lomonosov Moscow State University

Usp. Fiz. Nauk **110**, 623–668 (August 1973)

The present review is devoted to discussion of the principal stages of development of mirror electron microscopy. In the mirror electron microscope (MEM) the electron beam is reflected in a retarding electric field near the sample surface, and as a result the object being studied is not subjected to bombardment by the probe particles. This permits information to be obtained on the geometrical relief of the surface and the microfields in it. The review discussses the problems of MEM design, the different modes of operation, and questions of the limiting resolution. The theory of contrast formation for the geometrical relief and also for electric and magnetic microfields is discussed in detail. Experimental data are presented on investigation of a broad class of objects—semiconductors, dielectrics, and magnetic structures—in MEM. Various techniques for quantitative measurement of static and dynamic microfields on the surface of solid samples are described.

CONTENTS

1. Introduction 529
2. The Electron Mirror and the Mirror Electron Microscope 529
3. Design of Mirror Electron Microscopes 530
4. Modes of Operation of Mirror Microscopes 532
5. Imaging of Geometrical Relief and Electric Microfields 534
6. Resolution and Sensitivity of the Mirror Microscope 539
7. Imaging of Magnetic Microfields 542
8. Application of MEM in Physics Research 545
   a) Studies of Contact Fields and Semiconductors 545
   b) Studies of Dielectrics 547
   c) Visualization and Measurement of Magnetic Microfields 548
References 549

1. INTRODUCTION

The requirements of the developing field of semiconductor electronics and interest in surface physics are stimulating the perfection of electron-optical methods of studying various phenomena on solid surfaces. In addition to scanning electron microscopes,[1,2] emission microscopes,[3] and in some cases reflecting microscopes, wide application is being made of the mirror electron microscope (MEM),[5] which has a number of remarkable features. Only in this device is the object not subjected to bombardment by the probing particles but left undisturbed. In the MEM the electron beam is reflected in a retarding electric field near the surface of the sample, thus providing information on the geometrical relief of the surface and the microfields at the surface.

Mirror electron microscopes have a higher sensitivity to the geometrical relief of the surface studied and the electric microfields at the surface than do secondary-emission and scanning microscopes, since the probing electron is subjected to the action of the microfield twice—during retardation and during acceleration. In addition, only in the MEM is it possible, by controlling the potential difference between the electron gun cathode and the sample (the bias voltage), to study the distribution of the microfields at various heights above the surface. There is currently a trend to use these unique qualities of a mirror electron-optical system in combination devices—emission-mirror microscopes[6,7] and scanning-mirror microscopes.[8-10]

Reviews on mirror electron microscopy have already appeared in print. The review by Mayer[11] appeared more than ten years ago. In the article by Oman[12] little attention is given to the study of microfields. The book by Bok[13] and the review by Bok et al.[14a] are devoted mainly to description of the design of one type of MEM with a focused image and to certain questions of contrast formation in the image of electric microfields. The review article of Bethge and Heydenreich[15a] is concerned mainly with applications of mirror electron microscopy. None of the reviews except that of Mayer spend much time discussing the numerous articles on study of magnetic fields by means of MEM or questions of the theory of image formation in MEM. Theoretical investigations carried out recently have made it possible to use this device not only for qualitative observations but also to obtain quantitative data on microfields.

In addition to a rather large number of laboratory instruments of various types in existence, MEM are already being mass produced in Japan[14b] and Poland[16].

2. THE ELECTRON MIRROR AND THE MIRROR ELECTRON MICROSCOPE

An integral element of any MEM is the electron mirror, which plays a double role.[5] On the one hand, this is the most important part of the electron optics of the apparatus, which sometimes for this reason is called simply an electron mirror. On the other hand, the mirror electrode is also the object being studied. It is almost not bombarded by electrons, since it is at a small negative potential with respect to the electron gun cathode, and the electrons are reflected from an equipotential near the sample surface.

Electron mirrors have long been used in various electron-optical devices, and recently various attachments have appeared for electron microscopes, using the two main possibilities of electron mirrors: obtaining a mirror electron-optical image (real or virtual) of any object with simultaneous velocity filtering of the imaging

Copyright © 1974 The American Institute of Physics

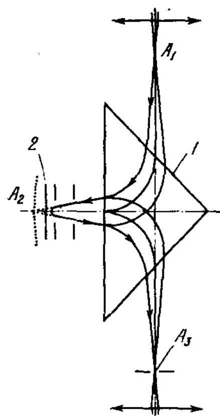

FIG. 1. Use of an electron mirror in a velocity analyzer. 1–Magnetic prism, 2–three-electrode mirror, A_1, A_2 –conjugate points.

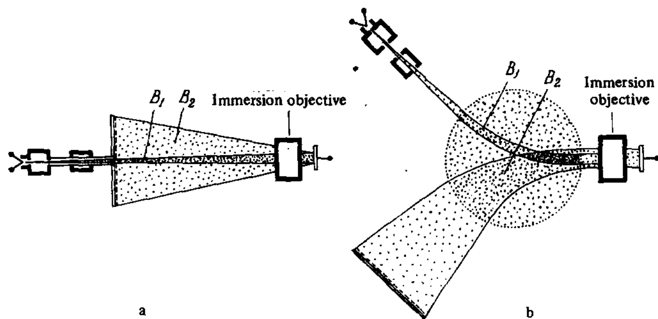

FIG. 2. Design variants of mirror microscopes.

electron beam. In particular, if the potential of the reflecting electrode with respect to the potential of the electron source is U_{bi}, only electrons with initial energy less than eU_{bi} will take part in formation of the mirror image (the remaining electrons will be absorbed by the reflector electrode).

As long ago as 1959 Vorob'ev[17] proposed use of an electron mirror as a filter for monochromatization of the electron beam in emission electron microscopes, which permits improvement of the resolution by several times. The practical realization[18] of this idea showed that the resolution of an emission microscope is actually improved. Mollenstedt and Gruner[18] mounted in an emission microscope an electron mirror with a magnetic prism to separate the incident and reflected beams (Fig. 1). A similar arrangement has been used in velocity analyzers in transmission electron microscopes[19-23] and in magnetic spectrometers (to reduce chromatic aberration).[24]

Electron mirrors are also used in image converters to transform an ion image to an electron image[25] (luminescent screens are destroyed under the action of ion bombardment), in electron-optical converters,[26,27] for focusing and modulation of beams in electron guns[28] (which permits improvement of the resolution and transmission of brightness gradations in transmitting and receiving television tubes), and in other devices.

The *first electron mirror* studied was a single lens which focused the transmitted electron beam for small negative potentials of the center electrode, but with increase of this negative potential was converted first to a converging mirror and then to a diverging mirror. The large chromatic aberration of such a lens did not permit a good mirror image[29] to be obtained, and therefore a two- or three-electrode mirror is usually used whose design is similar to that first developed by Hottenroth[30] except that diaphgrams are often used instead of cylinders (Fig. 1).

In studying the electron-optical properties of such mirrors, Hottenroth[30] noted that geometrical irregularities on the surface of the reflector electrode strongly perturbed an electron beam reflected near it, carrying an image of the subject (a grid). This observation also served as a stimulus for the development of electron mirror microscopy, the main problem of which is the study of surface structures: both the geometrical relief of a solid surface and various kinds of surface microfields. It should be noted that in study of specimens in MEM the microrelief of the surface can be formally assigned also to the category of microfields, but with the distinction that its existence and magnitude are due to the external field accelerating the electrons. Other microfields (p-n junctions, domain boundaries, magnetic and contact inhomogeneities, and so forth) can exist even in the absence of an external field.

The image of the surface nonuniformities is formed by a mirror electron-optical system whose design is usually the same as that of an immersion objective in emission electron microscopes,[31] and therefore MEM are sometimes considered as quasiemission systems.[32] The electron beam passes through the immersion objective twice: on the way to the sample and from it. Two variants[5] are possible for the path of the beam before the immersion objective (Fig. 2): either the axis of the reflected beam B_2 coincides with the axis of the illuminating beam B_1 (Fig. 2a) or the beams are separated by a magnetic field perpendicular to their axes (Fig. 2b). An instrument with separation of the beams is more complicated, but allows independent treatment of the illuminating and reflected beams.

3. DESIGN OF MIRROR ELECTRON MICROSCOPES

There are two main types of MEM—straight instruments in which the axes of the illuminating and imaging beams coincide, and instruments with separation of these beams (see Fig. 2). Instruments with beam separation were built first—the first laboratory glass models of

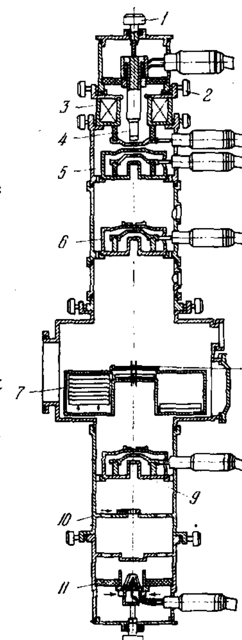

FIG. 3. Electron mirror microscope of the Electron Optics Laboratory, Moscow State University. 1–Mechanism for displacement of object in vertical direction, 2–mechanism for displacement of object in horizontal plane, 3–coil for magnetization and magnetic diaphragming, 4–object, 5–five-electrode immersion objective, 6–projection lens, 7–photographic chamber, 8–fluorescent screen for visual observation, 9–condenser, 10–gun diaphragm column, 11–electron gun.

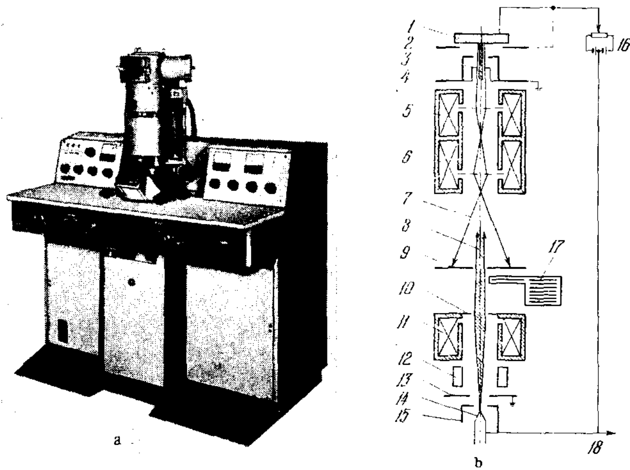

FIG. 4. External appearance (a) and beam path (b) in mass produced electron mirror microscope type JEM-M1 made by Jeol. 1–Sample, 2–screening electrode, 3–diaphragm, 4–anode, 5–intermediate lens, 6–projection lens, 7–reflected beam, 8–primary beam, 9–fluorescent screen, 10–diaphragm, 11–condenser lens, 12–adjusting coil, 13–gun anode, 14–heater, 15–oxide-coated cathode, 16–bias voltage source, 17–chamber for photographic plates, 18–to high-voltage source.

Hottenroth[30] and Orthuber[33], and the microscope of Bartz and co-workers[34,35] which had a resolution of 1000 Å. Subsequently Mayer[36] constructed the first straight instrument with a long-focal-length electron gun and a four-electrode immersion objective proposed earlier by Septier[37] for emission microscopes. The geometrical resolution of the instrument was about 0.35 micron.

A number of laboratory models of straight MEM have been built and used to observe the domain structure of ferroelectric and ferromagnetic crystals.[38-40] These instruments were the first to make use of a five-electrode immersion objective (sample + cathode diaphragm + isolated three-electrode lens), which permits easy transition from the diverging mode to the converging mode. The characteristics of the objective were investigated by Meshcheryakova.[41] A more refined laboratory MEM of straight design (Fig. 3) was described by Spivak et al.[42a]. The electron gun in this instrument is adjusted relative to the system axis, and the condenser is electrostatic. The microscope utilized a two-, three-, or five-electrode immersion objective (accelerating voltage 0–50 kV, vacuum to 10^{-6} mm Hg). In-vacuum photography is used also in a simpler device.[42b]

Straight MEM were constructed by Heydenreich and co-workers. A glass model[43] was first used, and then a metallic design.[44a] Use of a mirror inclined at a 45° angle to the system axis and located under a transparent luminescent screen permitted scale distortions to be avoided in external photography. A device for correction of the scale in photography has been described also by Szentesi[44b].

An MEM of straight construction with accelerating voltage up to 10 kV was built by Igras and Warminski[45] for investigation of semiconductors. The sample was grounded and its temperature could be varied over the range 77–1300°K.

The microscope with magnetic lenses constructed by Barnett and Nixon[46] uses a two-electrode mirror system (sample + diaphragm) with a magnetic objective lens and a double magnetic condenser. A two-lens projection system forms a distortion-free image in the region of magnification from 25× to 2500×. A similar device, the JEM-M1, has been developed and since 1968 has been mass produced by the firm of Jeol in Japan[14b,47]. In contrast to the Barnett-Nixon instrument[46], the Jeol microscope[14b] (Fig. 4) uses a three-electrode objective (sample + intermediate electrode + anode) and a chamber for in-vacuum photography on a flat film. The accelerating voltage is 15 or 35 kV (the stability is 3×10^{-4} min^{-1}), the vacuum is 5×10^{-5} mm Hg, and the resolution about 1000 Å.

A straight MEM with a vacuum of 10^{-7}–10^{-8} mm Hg was been described by Becherer et al.[48] The region near the sample is evacuated to an ultrahigh vacuum by an ion-sorption pump. The accelerating voltage is 1–30 kV, and the magnification up to 2000× (with an electrostatic projection lens).

In straight instruments a focused image cannot be obtained and the brightness of the shadow image is too low at large useful magnifications. Therefore interest has again risen recently in microscopes with separation of the beams. Mayer, who suggested MEM of straight construction, later built[49] an instrument with a total angle of separation of 30°. In this instrument the cathode of the electron gun is grounded, the sample is at a small negative or positive potential, and the column is at a high positive potential. Nevertheless the instrument is completely safe in operation, since all high-voltage parts are enclosed in protective plastic screens. The diaphragms of the four-electrode immersion objective are adjusted by means of precision glass tubes. All voltages are stabilized. The instrument is supplied with an automatic vacuum system and is equipped with remote control for displacement of the sample holder in three perpendicular directions.

A microscope of "classical" design (with grounded column) was built by Schwartze[50] in East Germany. The beams were separated by means of a magnetic prism with small astigmatism even for comparatively large deflection angles (the deflection angle in the instrument was 37.5°). The condenser and projection lenses were magnetic and of long focal length. The stabilized accelerating voltage was 6–36 kV, and the vacuum of the order 10^{-5} mm Hg. The mirror system was two- or three-electrode (the sample and the diaphragms). The maximum magnification of 2100× was achieved with a two-electrode mirror objective with a 1-mm diameter diaphragm located at a distance of 2 mm from the sample (the projection magnification was also maximal). The maximum field strength at the sample surface was 120 kV/cm. The resolution of the microscope was better than 2000 Å. It is possible to obtain both shadow and focused images of the sample surface.

In the much more complex instrument of Bok[13] with

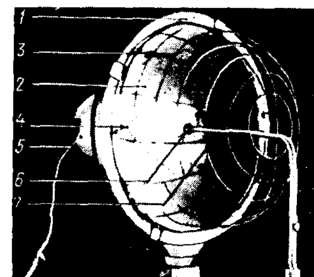

FIG. 5. Spherical mirror microscope. [53] 1–Outer sphere, 2–luminescent screen, 3–wire grid, 4–opening for primary beam, 5–electron gun, 6–sample, 7–holder.

beam separation, the imaging electron beam passes through four magnetic prisms which return it to the optical axis. The magnification of the focused or shadow images is 250× to 4000×. Use of four prisms with successive energizing of the windings permitted reduction practically to zero of the deflection chromatic aberration for a current stability almost two orders of magnitude poorer than with use of one prism. Deflection astigmatism is corrected by a stigmator installed at the last lens. The accelerating voltage is 0—30 kV.

The spherical electronic mirror[51-53] is incomparably simpler. For example, the instrument of Artamonov[53] (Fig. 5) easily achieves a high intensity of the retarding field near the object (up to 10^7 V/cm) without occurrence of breakdown, but in this microscope it is possible to obtain only shadow images and even these with a small field of view (comparatively large distortions occur even at small distances from the optical axis). Such an MEM is convenient as a simple and accessible laboratory instrument.

A microscope with beam separation for study of semiconductors has been constructed by E. Igras and T. Warminski (see ref. 16) and is mass produced in Poland. The main parameters of the instrument are: accelerating voltage 10—25 kV, working vacuum 10^{-5} mm Hg, magnification up to 2000×, resolution about 2000 Å; the sample temperature can be varied from 77 to 600°K.

The universal MEM with beam separation constructed by Heydenreich[54] was intended mainly for study of microfields and worked in the projection (shadow) mode, which provided maximum sensitivity to the fields. The large sample chamber made it possible to heat, cool, deform, or magnetize the sample to evaporate thin films onto it, to clean the surface by means of an ion gun, and to pass a controlled current along the sample surface. The accelerating voltage was 5—30 kV, the maximum magnification 3000×, and the resolution about 1000 Å. The instrument has been described in detail in an article.[15b]

At the present time various combination devices are being developed, including emission-mirror microscopes. One of the first microscopes of this type was built in Czechoslovakia.[6] With this microscope one can obtain thermionic, photoelectric, and field-emission images and mirror images of massive objects. A similar universal instrument was built in the USSR[7] on the basis of an ÉM-7 transmission electron microscope. This instrument uses a five-electrode immersion objective and an ion gun to obtain secondary-emission images. The authors[7] succeeded in obtaining a record resolution of 800 Å in a mirror image of a gold film.

Turner and Bauer[55] have briefly described an instrument which works as an emission, reflection, or mirror microscope and a low energy electron diffraction camera. This is the first MEM with ultrahigh vacuum (2×10^{-10} mm Hg). Samples in this microscope can be heated to 2800°K by an electron beam and cleaned by ion bombardment. Chang[56] used for low energy electron diffraction a very simple MEM with resolution of about 5 microns and magnification up to 1000×. The instrument worked as a spherical MEM, which provided preliminary charging of a small portion of the sample (dielectric substrate or film) by a fast electron beam, after which the electron energy was decreased and an electron-mirror image of the surface of the bombarded portion appeared at the spherical surface of the collector.

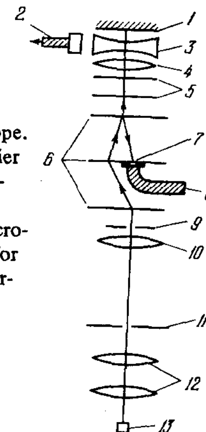

FIG. 6. Diagram of scanning mirror microscope.[60] 1—Sample, 2—scintillator and photomultiplier for ordinary scanning-electron-microscope operation, 3—equivalent diverging lens, 4—converging lens, 5—deflecting coils for scanning electron microscope, 7—contrast aperture with scintillator 8—for mirror scanning electron microscope, 9—lens aperture, 10—lens shaping the probe, 11—screen for observation in ordinary MEM operation, 12—reducing lenses, 13—electron gun.

An interesting combination of transmission and mirror microscopes was achieved by Kasper and Wilska[57], who developed an image brightness intensifier for a low-voltage transmission microscope. A weak image is recorded in the form of a potential relief on the reflecting electrode of an electron mirror, and this relief is then read by a much more intense electron beam. During the reading a magnetic prism is turned on which reflects the electron beam, and the instrument acts as an MEM with beam separation. The electron mirror also plays the role of an energy filter in recording images, if the potential of the reflecting electrode is close to that of the electron gun cathode.

A complex laboratory combined instrument developed by Nixon and co-workers[8] can be used as a transmission microscope, electron diffraction camera, emission microscope or mirror microscope.

A new device consisting of a combination of a mirror microscope with an electron diffraction camera for fast and slow electrons is being developed in France.[58,59] The vacuum in this device of the order 10^{-10} mm Hg, the accuracy in measurement of surface potentials 0.1 mV, and the localization about 10 microns. The apparatus consists of an electron gun, a magnetic deflecting prism, and two electron mirrors, one of which is intended for narrowing the energy spectrum of the reflected electrons (by approximately a factor of two) and the second for measurement of local potentials on the surface of the sample—the reflector of this mirror. Experiments are being carried out with a system consisting of three mirrors and a magnetic prism, which provides return of a monochromatized electron beam (after three reflections) to the initial axis.

Intensive development has also been carried out recently of scanning mirror microscopes,[10,60-63] which have all of the advantages of scanning electron microscopes[1] and are much more sensitive to surface microfields than ordinary scanning electron microscopes. Some of the instruments developed can be used also as ordinary mirror microscopes in which the image is formed all at once, rather than element by element (Fig. 6).

MEM can also be used for electron beam welding[64] with subsequent monitoring of the results in the mirror mode.

4. MODES OF OPERATION OF MIRROR MICROSCOPES

Two modes of operation are possible for MEM: the shadow (projection) mode and the focused mode.[65] In

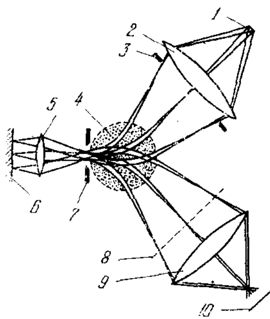

FIG. 7. Path of beams in mirror microscope with focused image. [65] 1–Electron source, 2–condenser lens, 3–viewing-field diaphragm, 4–magnetic prism, 5–objective, 6–object, 7–contrast diaphragm, 8–intermediate image, 9–projection lens, 10–final image.

the first case the image is formed in approximately the same way as in a shadow transmission electron (or optical) microscope, where a shadow image of the sample is produced by means of a real or virtual source of small size.[34] With illumination by a point source of electrons, in the geometrical-optics approximation each point of a uniform sample corresponds to a single ray and a definite point on the observation screen, and the screen can be at any distance from the sample. In practice this distance and consequently the useful magnification are determined by the size and brightness of the source.[66]

In operation in the focused mode the sample is illuminated by a beam with comparatively large aperture of the order of 10^{-2}–10^{-3} rad (the aperture in the shadow mode is usually less than 10^{-4} rad), in view of which each point of the sample corresponds already not to a ray but to a beam of electrons (Fig. 7), which after reflection is focused by an immersion objective. In this case a true stigmatic image is formed: each point of the sample corresponds to a conjugate point on the screen.

The focused mode cannot be achieved in a straight instrument with electrostatic lenses (see the diagram in Fig. 2a),[67] since, in view of the principle of reversibility of the path of the rays (the electron trajectories), the electrons illuminating a given point of the object would have to leave from the corresponding point of the image.[68a] To destroy the reversibility of the trajectories it is necessary to introduce a magnetic field. Then, even in a straight instrument, it is possible to use one half of the image plane for transmission of the illuminating beam. If magnetic quadrupole lenses are used,[69,70] it is possible to obtain imaging with magnification both of the source at the sample and of the sample at the screen. Then a small opening in the screen is sufficient for illumination, but other difficulties arise: Such imaging is possible only in the azimuthal direction; in the direction perpendicular to it the image is strongly demagnified, and therefore the illuminating beam must be scanned in a raster. The quality of the images in such a microscope is poorer than in the ordinary MEM.[13]

Obtaining a focused image is simplest in a microscope with beam separation.[65] The condenser lens in such an instrument (see Fig. 7) produces an image of the electron source in the focal plane of the objective, where the contrast diaphragm is located. The focal plane is imaged onto itself with a magnification of unity, since a ray from any point of this plane, after refraction in the converging objective lens, travels parallel to the optical axis, as reflected from the mirror-sample, and after a second refraction again hits the same point of the focal plane. Then the intermediate image produced by the objective is transferred to the final screen by the projection lens. The path of the illuminating beam between the illuminated field diagram and the sample is identical in a mirror sense to the path of the imaging beam between the sample and the plane of the intermediate image. This mode of operation of MEM is discussed in detail in the article by Schwartze[65] and the book by Bok.[13]

The imaging in a focused MEM is called quasiemission imaging, and this analogy is extended to the shadow mode of operation,[32] which, however, can be considered as simply a type of emission microscope without an aperture diaphragm in the strong-defocusing mode.[71a]

In spite of the large aperture of the beams, and consequently, the high brightness of the image in the focused mode, the shadow mode is often used in microscopes with beam separation, since in this case the sensitivity of the MEM to microfields at the sample is much greater. The image is produced by a two-electrode or three-electrode immersion objective and then magnified by subsequent electrostatic or magnetic lenses. The simplest two-electrode objective, which was used in early work in mirror microscopy,[35,72] provides a rather good image with a magnification of several hundred times (without an intermediate lens) and a resolution of about 1000 Å. The objective, which consists of the sample-reflector itself and the anode diaphragm (Fig. 8a), permits comparatively simple treatment of the main relations governing formation of electron-mirror images.[73,74] We will discuss the geometrical-optics characteristics of such an objective.

Let an electron source P_0 (the cross-over of the electron gun or its image formed by a condenser lens) with aperture $2\gamma_0$ and diameter $2\rho_0$ be placed a distance L_1 from a diaphragm A (Fig. 8b). It is possible to construct a virtual image P_1 of this source formed by the optical system consisting of the diverging lens A and the plane mirror K_1 located a distance $2l$ from it. Each point B of the sample K illuminated by the source P_0 (by a ray emitted from point B_0 parallel to the axis) corresponds (with a magnification of unity) to a point in the plane K_1 illuminated by the virtual source P_1. This source creates a shadow image of the plane K_1, and then the diverging lens A further magnifies this image. The combined action of the virtual source P_1 and the diverging lens A is equivalent, as can be seen from Fig. 8b and as follows from a simple calculation with the thin lens formula, to formation of a shadow image of the plane K_2 by another virtual source P_2, where plane K_2 is the image of the sample plane K with a magnification $M_2' = 2/3$.

Thus, instead of the shadow electron-mirror image of the sample plane K by the real electron source P_0, we can discuss the ordinary shadow image of plane K_2 by

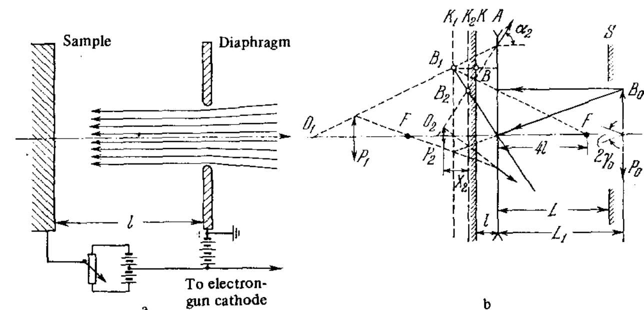

FIG. 8. Shadow operation of MEM with a two-electrode objective. a) Simplified diagram of two-electrode objective; b) design of source P_2 which accomplishes shadow projection of the sample plane.

the virtual source P_2 (in the approximation of geometrical optics). A simple calculation leads to the following values for the size of this virtual source $2\rho_2$, its distance x_2 from the imaged plane K_2, the aperture angle $2\gamma_2$, and the divergence $2\alpha_2$ (if we neglect the small convergence or divergence of the source P_0):

$$\rho_2 = M_2\rho_0,\ \mathrm{tg}\ \gamma_2 = \mathrm{tg}\ \gamma_0/M_2,\ x_2 = (4l/3)(1 - M_2),\ \mathrm{tg}\ \alpha_2 = 3\rho_0/4l, \tag{1}$$

where $1/M_2 = 2 + (3L_1/4l)$. Here the divergence $2\alpha_2$ of the source P_2 is understood to mean the opening angle of the cone of rays emitted from it for an aperture $\gamma_2 \to 0$. Since we are considering the approximation of paraxial optics, we can write $\tan\gamma \approx \gamma \approx \sin\gamma$.

For $L_1 \to \infty$ and $\gamma_0 \to 0$ (an infinitely distant point source P_0) the virtual source P_2 shifts to a point O_2 ($x_2 \to 4l/3$), and the magnification of the image at the screen S (for $L \gg l$) is $M = M_2'L/(4/3)l = L/2l$. The diameter of the illuminated region in plane K_2 in this case is determinated only by the divergence of the virtual source P_2 and is equal to $2\rho_0$, which corresponds to a portion of the sample with diameter $3\rho_0$—a factor of 1.5 larger than the beam diameter at the entrance to lens A.

The geometrical resolution δ of a shadow microscope depends on the size of the illuminating source and is approximately equal to its radius.[66] Therefore the resolution of a mirror microscope working in the shadow mode is determined by the size of the source P_2, and for $L_1 \gg l$ the distance resolved, referred to the sample plane, is

$$\delta \approx \rho_2/M_2' \approx 2(l/L_1)\rho_0. \tag{2}$$

For $L_1 \to \infty$ and ρ_0 = const, the resolution of MEM in the approximation of geometrical optics already is not limited by the electron source size $2\rho_0$. However, in the actual design of an instrument the ratio $l/L_1 \geq 5 \times 10^{-4}$, since usually $L_1 \leq 1$ m (it is determined by the permissible size of the instrument) and $l \geq 0.5$ mm (it is determined by the permissible electric field strength: for $l = 0.5$ mm and an accelerating voltage $U_0 = 10$ kV, the field strength at the sample surface is $E_0 = 200$ kV/cm, which is close to the breakdown value for ideal smooth surfaces). Therefore the limiting resolution of a shadow MEM (limited purely by geometrical factors) is $\delta \gtrsim 10^{-3}\rho_0$. At the present time a resolution of 800 Å has been achieved.[7] The resolution of focused MEM is still roughly the same. Theoretical limitations of the resolution will be discussed below.

It is not necessary to mix the converging and focused modes of operation of MEM. An ordinary straight instrument[75] can operate in the converging mode, for example, with a three-electrode objective (Fig. 9), but on focusing this objective onto the sample plane there is no image, for the reasons noted above. Thus, the converging mode, like the diverging mode, in a straight microscope is simply a variation of the shadow mode. The transition from the converging to diverging mode (with change of the electrode voltages of the three- or five-electrode objective) has been discussed in detail previously.[41,76a] A new design of five-electrode mirror objective has been described by Abalmazova.[76b]

5. IMAGING OF GEOMETRICAL RELIEF AND ELECTRIC MICROFIELDS

Surface relief or electric microfields at the reflector electrode distort the plane equipotential surfaces of the uniform retarding field of the immersion objective,

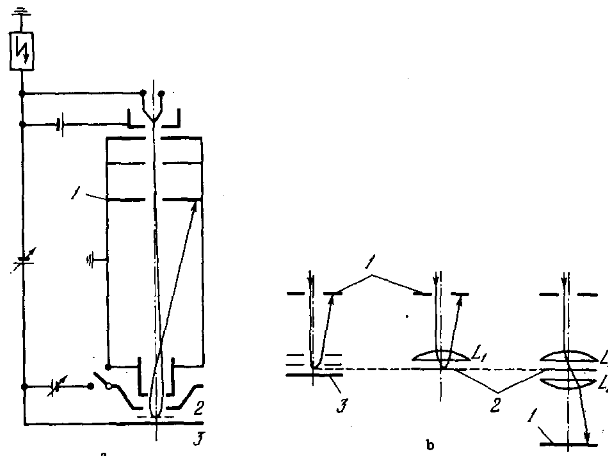

FIG. 9. Path of rays in converging mirror microscope (a) and its geometrical-optics analog (b). [75] 1—Screen for observation, 2—plane of reflection of rays or electrons, 3—sample.

which leads to velocity and density modulation of the reflected electron beam. Since a convex equipotential surface in the retarding field acts on the electrons in the same way as a diverging mirror on a light beam, a prominence on the sample surface will be reflected on the MEM screen (in the shadow diverging mode) in the form of a dark spot with a bright frame, while a depression or a positively charged region of the surface will focus the electron beam and a bright spot will appear on the screen.[33]

The problem of contrast formation in imaging of electric microfields was first discussed theoretically by Wiskott.[77] Starting with the postulates of geometrical optics, the author solves the problem of contrast in first order perturbation theory. A number of assumptions are made in the calculation: It is assumed that the field between the sample and the diaphragm of the two-electrode immersion objective (see Fig. 8a) is uniform, the primary beam is monochromatic, directed along the z axis, and remains parallel after passing through the diaphragm (a rather crude approximation, valid only in a very small region near the axis).

To find electron trajectories it is necessary to solve the equation of motion in the combined field $\mathbf{E}$ produced by the immersion objective and the microfields on the sample (in the half space $z \geq 0$):

$$\ddot{\mathbf{r}}(t) = \eta_0 \mathbf{E}(\mathbf{r}), \tag{3a}$$

$$\mathbf{E}(\mathbf{r}) = -\mathrm{grad}\,[E_\infty \cdot (z - z_0) + \psi(x, y, z)], \tag{3b}$$

where $\mathbf{r}$ is the electron radius vector, x and y are the coordinates in the sample plane (z = 0), and $\eta_0 = e/m$ is the charge-to-mass ratio of the electron. E_∞ is the intensity of the asymptotically uniform field of the objective, $\psi(x, y, z)$ is the potential taking into account perturbations at the sample surface, z_0 is the coordinate of the surface of zero total potential for the unperturbed field ($\psi \equiv 0$), i.e., the distance of this reflecting surface from the sample (z = 0). It is assumed that the geometrical size of the perturbations on the sample surface is much less than the distance from the sample to the diaphragm (then it is possible to introduce E_∞).

After calculation of the trajectories (for example, by numerical integration), the distribution of current density $j_z(x, y, z)$ is calculated in any cross section, proceeding from the conservation of tubes of current:

$$j_z\,df = j_{ze}\,df_e = \mathrm{const}, \tag{4}$$

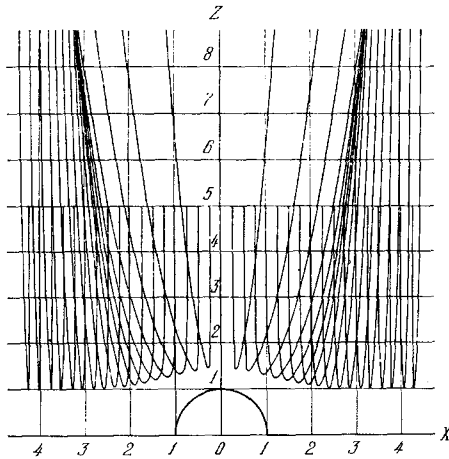

FIG. 10. Trajectories of electron reflected in the field of a hemispherical nonuniformity. Obtained by numerical integration of Eqs. (3a) and (3b) with introduction of dimensionless variables. A caustic figure [77] is formed at a distance $Z \approx 8$.

where j_{ze} is the current density of the illuminating beam and df_e is a surface element perpendicular to the axis of this beam. If we introduce generalized coordinates α and β and specify the electron trajectories in the form $\alpha = \alpha(\alpha_e, \beta_e, z)$, $\beta = \beta(\alpha_e, \beta_e, z)$ (the index e is for the entering beam), then

$$j_z/j_{ze} = df_e/df = [\partial(\alpha_e, \beta_e)/\partial(\alpha, \beta)]\, g(\alpha_e, \beta_e)/g(\alpha, \beta). \tag{5}$$

At all points of the surface

$$g(\alpha, \beta)\, \partial(\alpha, \beta)/\partial(\alpha_e, \beta_e) = 0 \tag{6}$$

the current-density component $j_z \to \infty$ (in the approximation of geometrical optics), i.e., a caustic figure occurs (Fig. 10).

In many cases, instead of numerical integration of (3a) and (3b), the trajectories can be found by the method of successive approximations, if we take as the zero approximation the trajectories in the unperturbed uniform field ($\psi = 0$). If the extent of the perturbing field in the z direction and its intensity are small, then according to Wiskott we can assume that the entire additional tangential impulse received by the electron in passing through the perturbation zone is applied at the turning point. This approximation is applicable as long as the tangential deflection of the electrons after traversing the perturbation zone is small in comparison with its dimensions.

If we neglect the z component of the perturbing field in comparison with the z component of the uniform field (i.e., if we assume that $\partial\psi/\partial z \ll 1$), then from (3a) and (3b) we can find a simple relation between the coordinate and time of the motion. In the dimensionless variables $X = x/a$, $Z = z/a$, $\Psi = \psi/aE$, $T = t(\eta_0 E_\infty/a)^{1/2}$ (a is a characteristic length, for example, the diameter of a depression in the sample), this relation has the form

$$T - T_0 = [2(Z - Z_0)]^{1/2}. \tag{7}$$

Then we can integrate Eq. (3a), for example, for the X coordinate:

$$\frac{dX}{dT}\Big|_a - \frac{dX}{dT}\Big|_e = \dot{X}_a - \dot{X}_e = \int_{-\infty}^{\infty} \frac{\partial\Psi(x, y, z)}{\partial X}\Big|_{\substack{X=X_e,\\ Y=Y_e}},$$
$$dT = 2\int_{Z_0}^{\infty} \frac{\partial\Psi}{\partial X}\Big|_{X_e,\, Y_e} \frac{dZ}{[2(Z-Z_0)]^{1/2}}; \tag{8}$$

here the index a refers to the departed (reflected) electrons. A similar relation can be written for the coordinate $Y = y/a$.

In this approximation (the entire tangential momentum is applied at the turning point) for a primary beam parallel to the axis ($\dot{X}_e = \dot{Y}_e = 0$) the reflected electron trajectories will be described by the relations

$$X_a(X_e, Y_e, Z) = X_e + [2(Z - Z_0)]^{1/2}\dot{X}_a(X_e, Y_e, Z_0),$$
$$Y_a(X_e, Y_e, Z) = Y_e + [2(Z - Z_0)]^{1/2}\dot{Y}_a(X_e, Y_e, Z_0). \tag{9}$$

Thus, for any given weak perturbation $\Psi(X, Y, Z)$, we can find the electron trajectories from Eqs. (8) and (9) and then calculate the current density in any cross section from Eq. (5). For example, for a perturbation in the form of a groove whose contour is given by the equation $Z - 2 + [Z/(X^2 + Z^2)] = 0$, the normalized equation of the trajectory obtained from (8) and (9) has the form

$$u_a = u_e - (\pi/Z_0^2)\, w^{1/2}\, [\sin((^3/_2)\,\mathrm{arctg}\, u_e)/(1 + u_e^2)^{3/4}], \tag{10}$$

where

$$u = X/Z_0 = x/z_0, \quad w = Z/Z_0 = z/z_0.$$

It is evident from this equation that for groove shapes of this type the trajectory shapes and consequently the shapes of the current-density distributions and caustic figures do not depend on Z_0 (if we do not take into account the extension in the direction of the z axis as a result of the coefficient Z_0^{-2} in Eq. (10)). Therefore, to find the current-density distribution in different sections, instead of mechanically displacing the screen in the z direction, we can utilize electrical displacement of the imaged surface if we vary the potential difference between the electron gun cathode and the sample being studied (the bias voltage). In particular, it is always possible to achieve incidence on the screen of sharp caustics corresponding to a Gaussian image of an infinitely remote emitting point. This conclusion has been confirmed experimentally by Wiscott and Bartz[35].

Representing the perturbation potential (for a two-dimensional problem) in the form

$$\Psi(X, Z) = \mathrm{Re}\int_0^{\infty} A(\tau)\exp(-\tau z - i\tau x)\, d\tau = \mathrm{Re}\sum_{n=0}^{\infty} \frac{A^n(+0)}{(Z + iX)^{n+1}}, \tag{11}$$

where

$$A^{(n)}(+0) = d^nA/d\tau^n\,|_{\tau\to+0}$$

(this representation is possible for a rather broad class of functions and satisfies the condition $\psi(x, z) \to 0$ for $z \to \infty$), Wiscott finds for the normalized velocity of the reflected electron

$$\dot{X}_a = \mathrm{Re}\frac{\sqrt{2}\pi}{i}\sum_{n=0}^{\infty} \frac{A^n(+0)}{Z_0^{n+3/2}}\, \frac{(2n+1)!}{2^n (n!)^2}\, \frac{1}{(1 + iu_e)^{n+3/2}} \tag{12}$$

(the three-dimensional problem is solved in a similar manner).

From this we can draw a conclusion which is important for the practical application of the mirror microscope: The electron trajectories on reflection at a large distance from the sample surface ($Z_0 \gg 1$) are determined mainly by the first nonzero term of expansion (12), i.e., by the large-scale imperfection of the sample structure. The fine structure becomes important only on reflection of electrons at a small distance from the sample surface. If it is necessary not only to observe but also to interpret the fine details, it is necessary to take care that they are not overlapped by the course structure, i.e., the surface should be well polished. In particular, Heydenreich[43,78a] showed that if the bias voltage is varied, it is impossible to obtain simultaneously sharp imaging (sharp caustics in the plane of the screen) of fine and coarse details of the relief. While light-optical imaging is two-dimensional (small depth of field), an MEM gives a spatial image of the relief, since the electron-optical refractive index $n \sim U^{1/2}$ varies smoothly.

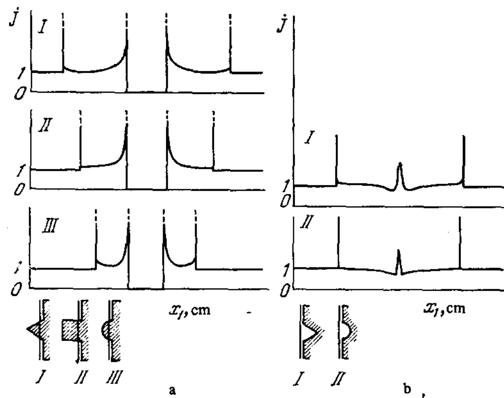

FIG. 11. Distribution of current density at the screen of an MEM, obtained in model apparatus [79] with reflection of electrons from projections (a) or depressions (b) of various shapes. The plane of reflection for a structureless object is shown by the straight line.

The method of calculating electron trajectories proposed by Wiscott has been carefully checked by Brand and Schwartz[79] in an apparatus which models the electron trajectories in MEM. A proportionally magnified object is probed by a thin parallel beam of electrons which is reflected near the geometrical nonuniformity being studied, accelerated in a uniform field produced by a system of cylindrical electrodes with increasing potential, and hits a luminescent screen. The dependence of the coordinate x_1 of the point of incidence on the screen on the coordinate x_0 of the point of entry of the beam is found. The current density i which would arise at the corresponding portion of the MEM screen is found as the ratio dx_0/dx_1. If the turning point is at some distance from the object, Wiskott's method gives a sufficiently good approximation (the agreement of the measured and calculated curves is quite satisfactory). For close reflection, as we should expect, the agreement is poorer. Brand and Schwartze[79] reached the conclusion that it is difficult with a mirror microscope to distinguish the shape of geometrical projections (or depressions) on the sample surface, since the images of projections (depressions) of radically different shape are almost the same (Fig. 11).

From the calculation presented above it follows that the contrast of images of geometrical relief and electrical nonuniformities is determined by the same equations if corresponding perturbation potentials are introduced. Thus, a great similarity exists in the mechanisms of formation of mirror images of geometrical relief and electrical microfields. This has been emphasized by Heydenreich[78b] in the case of images of cleavage steps and potential jumps. Since a geometrical or electrical step of this type can be considered as a concavo-convex irregularity, its image will be a double light-dark band whose light edge corresponds to the more positive (or lower) portion of the surface (Fig. 12). This band, in addition, is displaced in the direction of the lower level (higher potential). Therefore mirror images of projections are drawn out and those of depressions are compressed (Fig. 13). A similar distortion in the image of a sinusoidal potential has been discussed by Barnett and England[80]. When a current flows along the sample surface, portions with good conductivity are distinguished in relief in the image in the form of dark regions with a white edge and appear raised slightly above portions with poorer conductivity: it is possible to take unique stereoscopic pictures in which the stereoscopic effect is achieved by a simple variation of the currents through the sample.[81]

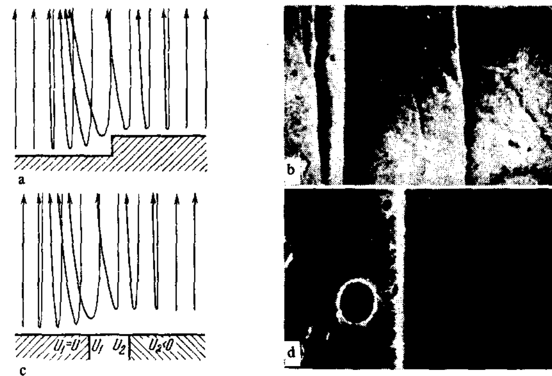

FIG. 12. Image of geometrical (a, b) and electrical (c, d) steps on a sample surface.

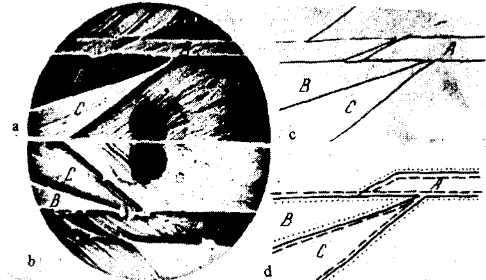

FIG. 13. Image of steps on a cleavage surface in NaCl. a, b) Electron-mirror image of corresponding cleavage surfaces; c) optical image; d) drawing of the displacement of the mirror image of the steps (dashed line) with respect to the optical image (solid lines).

In spite of the great similarity in formation of the images of electric microfields and geometrical relief, there is a difference between them which is important for practical applications: the geometrical contrast improves with increasing field strength E_∞ of the retarding field, while the electrical contrast becomes poorer. This can be seen directly from the equation for increase of the tangential momentum of the electron (8), where $\Psi = \psi/aE_\infty$, and the potential ψ is bounded for the electrical nonuniformity. This effect of suppression of the electrical microlens by the microlens of the accelerating field of the immersion objective was pointed out in refs. 45 and 82. The action of the electrical microlens is discussed qualitatively also in an article by Spivak et al.[83]

A more rigorous theoretical approach to the problem of contrast in electric microfield images is given by Sedov et al.[84] on the basis of the general method for solution of contrast problems.[71b] Wiskott's method is used to calculate the electron trajectories, but the perturbing potential $\psi(x, y, z)$ is represented not by expansion (11) but in the form of an integral—as the solution of a Dirichlet problem for the half space $z \geq 0$ with the boundary condition $\psi(x, y, 0) = \varphi(x, y)$ (where $\varphi(x, y)$ is the specified potential on the sample surface):

$$\psi(x, y, z) = (z/2\pi) \int\int_{-\infty}^{\infty} \{\varphi(x-\xi, y-\eta)/[\xi^2+\eta^2+z^2]^{3/2}\}\, d\xi\, d\eta. \quad (13)$$

After substitution of ψ into an equation such as (8) we can find the increase $\Delta \mathbf{v}$ in the tangential velocity of an electron reflected directly from the sample surface and which has passed through the region of influence of a perturbing microfield:

$$\Delta v = \{(2\pi\eta_0/E_0)^{1/2}/[\Gamma(1/4)]^2\} \int\int_{-\infty}^{\infty} [\text{grad}\, \varphi(x-\xi, y-\eta)/(\xi^2+\eta^2)^{3/4}] d\xi\, d\eta; \quad (14)$$

here E_0 is the intensity of the uniform retarding field (it corresponds to E_∞ in Eq. (3b)) and $\Gamma(1/4) \approx 3.626$. We can then calculate the corresponding displacement of the point of incidence of the electron on the microscope screen. For example, for an MEM with a two-electrode objective in the shadow mode, the radial displacement is[84]

$$\Delta R = (\Delta v/v_0)3L/2, \quad (15)$$

where $v_0 = (2\eta_0 U_0)^{1/2}$ is the electron initial velocity, $U_0 = E_0 l$ is the accelerating voltage, l and L are respectively the distances from the immersion objective anode to the sample and screen. The image contrast, i.e., the current density distribution on the screen, is calculated from an equation similar to (5).

For a one-dimensional microfield on the surface we obtain Δv from Eq. (14) by integration over η. If the electron is reflected at some height h above the sample surface, then

$$\Delta R = \frac{3Ll^{1/2}}{2^{3/2}U_0} \int_{-\infty}^{\infty} \frac{d\varphi(x-\xi)}{dx} \left[\frac{h+(\xi^2+h^2)^{1/2}}{\xi^2+h^2}\right]^{1/2} d\xi. \quad (16)$$

The height of reflection h above a sample point located a distance r from the optical axis is determined by the approximate formula

$$h = (r^2/36l) + (U_{bi}/U_0)l, \quad (17)$$

where U_{bi} is the bias voltage.

If the perturbing field potential depends only on one coordinate x in the sample (X on the screen), we can write the condition of conservation of tubes of current (4) in the form

$$j_0(X)\, dX = j(X')\, dX', \quad (18)$$

where $j_0(X)$ and $j(X')$ are the initial and perturbed current densities on the screen, X' is the new coordinate of the point of incidence of the electron on the screen in the presence of the perturbation, where

$$X' = X + S(X); \quad (19)$$

here $S(X) \equiv \Delta X(X)$ denotes the magnitude of the shift of the point of incidence of the electron on the screen. From Eqs. (18) and (19) it follows that

$$j(X') = j_0(X)\{1 + [dS(X)/dX]\}^{-1}. \quad (20)$$

From the contrast pattern, i.e., from a known function $j(X')$, it is possible to reproduce the microfield which produced the contrast. Here the problem is broken down into two steps: 1) finding the displacement of the electrons S(X) under the influence of the microfields for a given distribution $j(X')$; 2) calculation of the microfields from the calculated displacement S(X). Several different methods exist for solution of the first part of the problem. We mention first the graphical method.[84] Integrating Eq. (18), we obtain

$$I_0(X) = \int_{X_0}^{X} j(X)\, dX = \int_{X_0'}^{X} j(X')\, dX' = I_1(X'). \quad (21)$$

Equating integrals I_0 and I_1, we find S(X) (Fig. 14). The displacement, referred to the sample, is $\Delta x(x) = S(X)/M$, where M is the magnification of the instrument. Unique determination of S(X) is possible only if there are no caustic lines in the image, i.e., if the condition $dS/dX > -1$ which follows from Eq. (20) and is analogous to condition (6) is satisfied at all points of the image. A method close to that discussed above was used by Cohen and Harte[85], who determined the displacement from equations similar to (21) but by computer

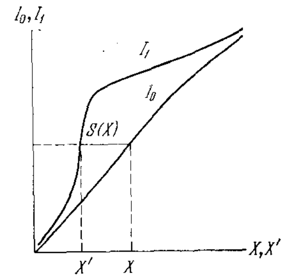

FIG. 14. Determination of the displacement S(X) of the point of incidence on the screen of an electron which has passed through the region of action of a perturbing microfield. I_0—integral distribution curve of current density at the screen in the absence of a perturbing microfield, I_1—integral curve with microfield turned on.

rather than graphically. In addition, Gvozdover[86] has suggested a method of automatic recording of the displacement S(X) based on introduction of a negative feedback circuit in the deflection system of the MEM. Sedov[87] obtains relations similar to (21) for two-dimensional microfields with circular symmetry. The quantity S(X) can be found also by direct measurement of the displacements in the image, for example, of a fine coordinate grid deposited on the sample surface.

If the trajectory displacement is measured, it is possible by solution of an integral equation similar to (16) by computer to calculate the distribution of potential. Equation (16) is an integral equation of convolution with respect to the function $d\varphi/dx$. If we apply the Fourier transform method, with regularization of the divergent interval, to Eq. (16), we can find (for h = 0) the solution of the inverse contrast problem[88]:

$$d\varphi/dx = (U_0/3\cdot 2^{1/2}\pi L l^{1/2}) \int_{-\infty}^{\infty} \{[\Delta R(x) - \Delta R(x-\xi)]/|\xi|^{3/2}\} d\xi. \quad (22)$$

Thus, if we find from the current density distributions on the MEM screen (with the microfield turned on and turned off) the displacement of the electron trajectories under the influence of the microfield, we can calculate by computer the field $d\varphi/dx$ and the potential $\varphi(x)$ at the sample surface or at any height h above it. The solution obtained for the inverse problem demonstrates a weak instability.[88] For $h \neq 0$ the inverse problem must be solved with regularization by the method of Tikhonov.[89]

The contrast of geometrical relief images is calculated with the same approximations,[71] since a projection of height h on the sample surface in a uniform field E_0 is equivalent to reduction of the potential of a given portion of the surface by an amount $(-E_0 h)$, i.e., it is possible to replace the geometrical relief function h(x, y) by an electrical relief, a potential distribution of the form

$$\varphi(x, y) = -E_0 h(x, y) \quad (23)$$

and then carry out the calculation of contrast with Eqs. (16)—(20).

A somewhat different approach to the problem of imaging potential and geometrical reliefs in MEM, developed recently by a number of investigators,[90-93] is the method of spectral characteristics. The mirror electron-optical system is considered as a certain filter which provides a more or less distorted transmission of the spectrum of spatial frequencies at the sample, much an an ordinary radiofrequency filter transmits various bands of time frequencies. Therefore the determination of sensitivity and contrast of an image produced by a mirror electron-optical system reduces to finding its transmission spectrum or, more precisely, to finding its frequency-contrast (spectral) characteristic.

The potential distribution at the sample surface can be represented in the form of a Fourier integral (we consider the one-dimensional case):

$$\varphi(x) = (1/2\pi)\int_{-\infty}^{\infty}\varphi_0(\omega)\exp(i\omega x)\,d\omega,\quad \varphi_0(\omega) = \int_{-\infty}^{\infty}\varphi(x)\exp(-i\omega x)\,dx, \tag{24}$$

where $\omega = 2\pi\nu = 1/a$ is the spatial frequency of the signal ($2\pi a$ is the spatial period), $\varphi_0(\omega)$ is the spectral density of the potential relief (the amplitude of the potential for a sinusoidal potential distribution).

If the imaging system is linear, i.e., if its parameters do not depend on the amplitude of the initial signal, the brightness distribution on the screen j(x) of this idealized system or the relative contrast of the image K(x) can be represented in the form[91]:

$$K(x) = [j(x) - j_0]/j_0 = (1/2\pi)\int_{-\infty}^{\infty}\varphi_0(\omega)S(\omega)\exp[i\omega x + i\Omega(\omega)]\,d\omega, \tag{25}$$

where the image spectrum is equal to the product of the initial spectrum $\varphi_0(\omega)$ and the spectrum of the transmission system $S(\omega)$. If the spectral characteristic of the system $S(\omega)$ and the phase-frequency function $\Omega(\omega)$ are known, Eqs. (24) and (25) can be used to calculate the contrast of the image of an arbitrary potential distribution at the sample. For a sinusoidal distribution of the potential studied, the spectral characteristic is the coefficient of the transformation of the relief amplitude into the contrast amplitude.

The process of image formation, discussed from the point of view of transmission of information on the sample structure, can be broken into three stages: 1) modulation of the information carriers (electrons) by the structure being studied, 2) transmission of the information, and 3) demodulation. In an emission microscope with an aperture diaphragm and in an MEM with a focused image, demodulation is accomplished by cutting off the deflected electrons by the edge of the diaphragm, and in a shadow MEM it takes place simultaneously with transmission of the information: the electron beam modulated in velocity by the relief being studied is redistributed in density. Both forms of demodulation are linear only in a narrow range of degree of modulation, shadow imaging being the more sensitive means of demodulation.[90] The efficiency of modulation in various systems has been discussed in detail by Artamonov.[94]

The transfer function (the spectral characteristic) for shadow MEM was first discussed by Schwartze,[90] but a much more complete solution was obtained by Artamonov and co-workers (see refs. 91 and 94) and later in somewhat simplified form found independently by Barnett and Nixon.[93] The method of solution employed by Barnett and Nixon[93] is as follows. For a symmetric perturbing potential at the surface, depending only on the coordinate x, the potential distribution is found (as a solution of Laplace's equation) in the half-space above the sample for $z \geq 0$:

$$\varphi_\mu(x, z) = (1/\pi)\int_0^{\infty}\varphi_0(\omega)\exp(-\omega z)\cos\omega x\,d\omega. \tag{26}$$

The method of successive approximations is then used to solve Eqs. (3a) and (3b), i.e., the displacements $s = x - x_0$ of the electron trajectory under the influence of the microfield are found. For small s and ds/dx the relative contrast of the image is $K(x) \approx -ds/dx$. Since the equations of motion are nonlinear, the image contrast found in the form (25) will contain nonlinear functions

$$S = S(\omega, \varphi_0(\omega)) \text{ and } \Omega = \Omega(\omega, \varphi_0(\omega)).$$

However, for weak microfields whose intensity $\mathbf{E}_\mu$ satisfies the *condition*

$$|\mathbf{E}_\mu|_{\max} \leqslant 0{,}3\ E_0, \tag{27}$$

and for a frequency band bounded on the low side (we do not consider microfields whose period is greater than the sample size or the sample-screen distance), the nonlinearity is small, and therefore the rather complex expression for the contrast is simplified, the function $\Omega(\omega)$ can be neglected, and the spectral characteristic of the mirror system (in the interval $\omega_0 \leq \omega \leq 0.1\,\omega_{\mathrm{lim}}$) takes the *form*

$$\begin{gathered} S(\omega) = \pi\omega^{3/2}\{E_0\sqrt{\omega_0}[1 - (2\alpha E_\mu^0/\pi E_0)]\}^{-1}\exp(-\omega\delta), \\ E_\mu^0 = \frac{1}{\pi}\int_0^{\infty}\omega\varphi_0(\omega)\exp\left(-\omega\frac{U_{\mathrm{bi}}}{E_0}\right)\cos\omega x_0\,d\omega,\quad \delta(x_0) \\ = \frac{U_{\mathrm{bi}}}{E_0}\,\frac{1 - 2\alpha(E_\mu^0/\omega U_{\mathrm{bi}})}{1 - 2\alpha(E_\mu^0/\pi E_0)}; \end{gathered} \tag{28}$$

here $\alpha \approx 0.6$ is the coefficient of the quadratic approximation of the nonelementary functions describing the solution of the equations of motion, $\delta(x_0)$ is the equation of the equipotential for reflection of the incident electrons, $\omega_0 = \pi/L$, L is the distance from the reflection equipotential to the plane of the screen (located, according to the condition, in the same uniform field), $\omega_{\mathrm{lim}} = \pi E_0/\varphi_0$ is the limiting frequency of a signal with amplitude φ_0 reproduced by the mirror system. The limitation $\omega \leq 0.1\,\omega_{\mathrm{lim}}$, as can easily be shown for a sinusoidal distribution, is equivalent to condition (27) that the microfield be small.

The spectral characteristic (28) can be calculated for an arbitrary field distribution at the sample and a monokinetic illuminating beam. In practice it is better to use the spectral characteristic for a sinusoidal distribution, since otherwise the reflection equipotential $\delta(x_0)$ which depends on the signal frequency ω loses its physical meaning. In addition, when condition (27) is taken into account, for sufficiently high bias voltage $U_{\mathrm{bi}} > E_0/\omega_0$ the expression for the spectral characteristic can be simplified:

$$S(\omega) = [(\pi L)^{1/2}/E_0]\,\omega^{3/2}\exp(-\omega U_{\mathrm{bi}}/E_0).$$

A similar expression for the spectral characteristic was also obtained less rigorously by Barnett and Nixon[93] with the same approximations but with inclusion of the geometrical optics of a real mirror microscope:

$$T(\nu) = A\nu^{3/2}\exp(-2\pi\nu U_{\mathrm{bi}}/E_0) \tag{29}$$

($\nu = \omega/2\pi$ is the spatial frequency, $T(\nu)$ is the transfer function for low contrast, A is a parameter which depends on the geometrical optics of the system and the retarding field intensity). The spectral characteristic (Fig. 15) has a maximum for $\nu_{\max} = 3E_0/4\pi U_{\mathrm{bi}}$. With decreasing bias voltage (or with increasing field intensity E_0) the optimal spatial period, which gives the maximum image contrast, decreases, i.e., the resolution of the instrument improves. However, for small U_{bi} in a real instrument, the fast electrons from the Maxwellian tail of the velocity distribution hit the sample surface and therefore the contrast and resolution are spoiled.

The effect of the spread in velocities kT/e of the illuminating beam on the form of the spectral characteristic has been studied by Artamonov and Komolov.[91] For a sinusoidal distribution of potential at the sample and a Maxwellian distribution of velocities of the illuminating beam

$$S(\omega) = \frac{\omega^{3/2}}{E_0\omega_0^{3/2}}\exp\left(-\omega\frac{U_{\mathrm{bi}}}{E_0}\right)\frac{\exp[-(\omega^2\pi/E_0\omega_0 M^2)\,kT/e]}{[1 + (\omega/\pi E_0)\,kT/e]^{1/2}}$$

(M is the magnification of the instrument, $\omega = \pi/\mathscr{L}$, $\mathscr{L}$ is

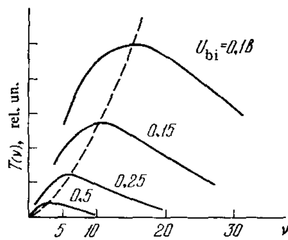

FIG. 15

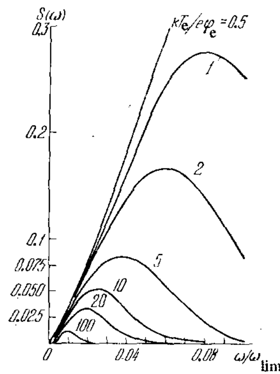

FIG. 16

FIG. 15. Spectral characteristics of MEM (in relative units) for various bias voltages U_{bi} for an accelerating field strength $E = 2\pi$ V/μ ≈ 62.8 kV/cm. The dashed curve shows a plot of the function $T(\nu_{max}) \alpha \nu_{max}^{3/2}$.

FIG. 16. Spectral characteristics for different velocity spreads of the illuminating beam $kT_e/e\phi_e$. [91].

the sample-screen distance). The nonmonokineticity of the beam leads to a drop in the spectral characteristic at high frequencies (Fig. 16), i.e., to a deterioration of the resolution of the mirror system.

An error should be noted in the work of Barnett and Nixon.[93] The spectral characteristic (see Fig. 15) in the region $\nu \gtrsim \nu_{max}$ can be used only for very crude estimates, since in this region (for a fixed amplitude of the harmonics of the potential distribution) condition (27) for smallness of the microfield is not satisfied; it is this condition which permits the equations of motion of the electron to be linearized and Eq. (29) to be obtained. For just this reason the spectral characteristic in refs. 91 and 94 is constructed only in a narrow range of frequencies (compare Eq. (28) and Fig. 16). Bok et al.[95] note another inaccuracy in the work of Barnett and Nixon[93]: Eq. (29) does not contain a factor of the form $\exp(-2\pi\nu E_\nu/E_0)$ which enters implicitly in Eq. (28) and also leads to a nonmonotonic dependence of the spectral characteristic on frequency. The spectral characteristics for MEM operating in the focused mode were obtained for the first time by Schwartze[65] and have been discussed in more detail in the article by Bok et al.[95] and in Bok's book.[13]

As a consequence of the very substantial nonlinearity of the mirror system, the behavior of the spectral characteristic is different for positive and negative portions of the potential relief (the shift of the image toward the more positive portions—see above), and therefore it is necessary to construct an averaged spectral characteristic, which of course reduces the advantage of the method being discussed. Nevertheless the experimental verification of the theoretical values of the spectral characteristic, carried out by Artamonov and coworkers[92], showed a quite satisfactory agreement of the theoretical and experimental data.

Thus, a real mirror electron-optical system can also (with certain assumptions) be considered as a quasilinear filter of spatial frequencies with a limited pass band (a strong falloff at high and low frequencies).

We must also point out[96] the similarity of the two apparently different methods presented above for solving the problem of contrast in the image of electric microfields. If we carry out a Fourier transformation of an integral expression of the convolution type (13), we obtain for a one-dimensional potential distribution on the surface a potential representation similar to (26), which shows the similarity of the initial stages of the two means of determining the image contrast.

6. RESOLUTION AND SENSITIVITY OF THE MIRROR MICROSCOPE

A rigorous solution of the problem of the limiting resolution δ of a mirror microscope can be obtained only from the point of view of wave mechanics, since at the turning point the De Broglie wavelength $\lambda \to \infty$. A rough estimate of δ can be obtained quasiclassically from the Heisenberg uncertainty relation (see ref. 77). For example, for a periodic potential distribution at the sample (a spatial period $2\pi a$ in x and y)

$$\begin{aligned}\Psi_0 &= (1/2)\exp[-(z/a)-1][\cos(x/a)+\cos(y/a)]\\ &= (1/2)\exp[-(Z+1)](\cos X+\cos Y)\end{aligned} \quad (30)$$

the increase in tangential velocity, in agreement with Eq. (8), is

$$\Delta\left(\frac{dX}{dT}\right)=2\int_{Z_0}^{\infty}\frac{\partial\Psi_0}{\partial X}\Big|_{X_e}\frac{dZ}{[2(Z-Z_0)]^{1/2}}=-\left(\frac{\pi}{2}\right)^{1/2}\exp(-Z_0-1)\sin X_e$$

and the maximum increase of momentum is $\Delta p = (\pi m a e E_\infty/2)^{1/2}\exp(-Z_0-1)$.

A "picture" of the sample surface appears if the deflection Δs of the imaging electrons is no smaller than the extent of the perturbation region. From the Heisenberg relation $\Delta p \Delta s \geq \hbar/2$, if we set $\Delta s = 2\pi a$ and use the value of Δp found above, we can find the resolvable period:

$$\delta = 2\pi a \geqslant \exp[(2/3)(Z_0+1)](\hbar^2/meE_\infty)^{1/3}. \quad (31)$$

For $z_0 = 0$ (reflection directly from the perturbed sample surface) and E_∞ = 100 kV/cm the minimum resolvable spatial period according to Eq. (31) is $2\pi a_{min} \approx 40$ Å. According to the more accurate evaluation of Wiskott, $2\pi a_{min} \approx 70$ Å.

An analysis of the limiting resolution of an idealized MEM without taking into account geometrical-optics limitations has been carried out by Wiskott.[77] The method of successive approximations was used to solve the Schrödinger equation for the wave function U, which in normalized form can be written

$$\Delta U + (9/4)[\zeta + \alpha\Psi(\xi,\eta,\zeta)]U = 0, \quad (32)$$

where

$$\xi = x/l_0,\ \eta = y/l_0,\ \zeta = (Z - Z_0),\ \alpha = a/l_0,\ \beta = b/l_0,\ l_0 = (9\hbar^2/8emE_\infty)^{1/3}.$$

For a periodic potential distribution

$$\Psi(\xi,\eta,\zeta) = \sum_{\mu,\nu} v_{\mu\nu}\exp\{-(\zeta+\zeta_0)[(\mu^2/\alpha^2)+(\nu^2/\beta^2)]^{1/2}\}\exp\{i[\mu(\xi/\alpha)+\nu(\eta/\beta)]\} \quad (33)$$

(the periods along the x and y axes are respectively $2\pi l_0\alpha$ and $2\pi l_0\beta$; the coefficient $v_{00} = 0$, and the remaining coefficients are arbitrary) the wave function is sought in the form

$$U(\xi,\eta,\zeta) = \sum_{\mu,\nu} U_{\mu\nu}(\zeta)\exp\{i[\mu(\xi/\alpha)+\nu(\eta/\beta)]\}. \quad (34)$$

After substitution of (33) and (34) into (32), we obtain for the coefficients $U_{\mu\nu}$ an inhomogeneous Bessel equation which is integrated by the method of successive approximations if we assume that $\alpha < 1$ is the small parameter. The image contrast, i.e., the ratio of the current density

$j_{\zeta a}$ of the reflected electrons to the current density $j_{\zeta e}$ of the incident parallel monochromatic beam (a plane wave), is then found as the ratio

$$j_{\zeta a}/j_{\zeta e} = |U_a|^2/|U_e|^2.$$

For the simplest periodic potential distribution $\Psi = \Psi_0$ according to Eq. (30) ($a = b$, $v_{\mu\nu} = 1/4e$ for $\mu^2 + \nu^2 = 1$ and $v_{\mu\nu} = 0$ for $\mu^2 + \nu^2 \neq 1$) the first approximation for solution of the Bessel equation gives

$$j_{\zeta a}/j_{\zeta e} = 1 + (8/3)\,|C^{(1)}_{10,a}|\,[\cos(\xi/\alpha) + \cos(\eta/\alpha)]\sin(2\zeta^{1/2}/3\alpha^2).$$

The coefficient $C^{(1)}_{10,a}$ of the first approximation and the coefficients $C^{(2)}_{\mu\nu,a}$ of the second approximation are given in Fig. 17 as a function of $2\pi\alpha$. Taking as a criterion of resolution of a periodic structure the ratio of minimum current density to maximum current density

$$j^{\min}_{\zeta a}/j^{\max}_{\zeta a} = [1-(16/3)\,|C^{(1)}_{10,a}|]/[1+(16/3)\,|C^{(1)}_{10,a}|] \leqslant 3/4,$$

we obtain a limit for the coefficient $4|C^{(1)}_{10,a}| \geq 3/28$ and from Fig. 17 (for $\zeta_0 = 0$) we find the minimum resolvable period:

$$2\pi a_{\min} \approx 3.45\,(9\hbar^2/8emE_\infty)^{1/3}. \qquad (35)$$

For $E_\infty = 100$ kV/cm in an ideal MEM a structure with a period of about 70 Å should be resolved, and in a proton mirror microscope—about 6 Å.

A peculiar anisotropy of the resolution of MEM should be noted. The instrument resolves a step of very small height—less than the transverse resolution $2\pi a_{\min}$. In particular, let us designate by $\Delta\zeta = \Delta z/l_0 = \alpha\Delta Z$ the difference between the maximum and minimum heights (extent in the z direction) of the equipotential surface from which the electrons are reflected:

$$\Phi = (\zeta/\alpha) + \Psi_0 = (\zeta/\alpha) + (1/2)\exp[-(\zeta_0+\zeta)\alpha^{-1} - 1]\,[\cos(\xi/\alpha) + \cos(\eta/\alpha)] = 0,$$

or

$$Z - Z_0 + (1/2)\exp[-(Z+1)]\,(\cos X + \cos Y) = 0.$$

Computing $\Delta\zeta$, we find that for various $\zeta_0 = z_0/l_0$ (see Fig. 17) the transverse resolution $\Delta x_{\min} = 2\pi a_{\min}$ and longitudinal resolution $\Delta Z_{\min} = l_0\Delta\zeta$ given in Table I are obtained.

In the table for $E_\infty = 100$ kV/cm and $l_0 = 20.5$ Å we have given approximate numerical values of resolution (in Å), bias voltage $U_{bi} = E_\infty z_0 = E_\infty l_0\zeta_0$, and the potential amplitude at the surface (in mV):

$$|\psi_0|^{\max}_{z=0} = aE_\infty|\Psi_0|^{\max}_{z=0} = (\Delta x_{\min}/2\pi\cdot 2.718)\,E_\infty \approx 0.06\Delta x_{\min}\cdot E_\infty. \qquad (36)$$

Thus, in an ideal MEM for a sufficiently high retarding field strength E_∞ it is possible by choice of the appropriate bias voltage to observe geometrical steps on the sample surface of height several angstroms (without substantial deterioration of the transverse resolution $\Delta x_{\min}$) or a sinusoidal potential distribution with amplitude several millivolts. However, the voltage sensitivity of the instrument decreases with increasing E_∞: it follows from (35) and (36) that the detectable potential amplitude $|\psi_0|^{\max} \sim E^{2/3}$. The anisotropic resolution of a mirror microscope has been confirmed experimentally: Bartz, Weissenberg, and Wiskott[35] obtained an image of a lattice with a feature depth of 25 Å (Fig. 18) in an instrument with a transverse resolution of about 1000 Å, and Mayer[11] observed a step on the cleavage surface of a single crystal of barium stearate of height 24.4 Å. The electron-mirror interferometer[97] provides the possibility of measuring the height of steps with an accuracy as low as 0.05 Å.

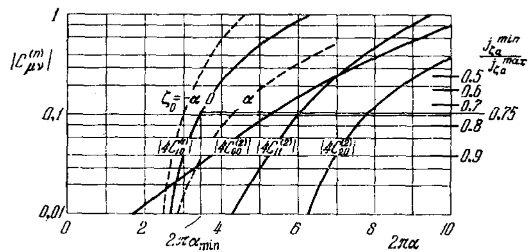

FIG. 17. Coefficients $C^{(n)}_{\mu\nu,a}$ of the series expansion of the wave function, and image contrast for a periodic potential distribution at the sample. [77]

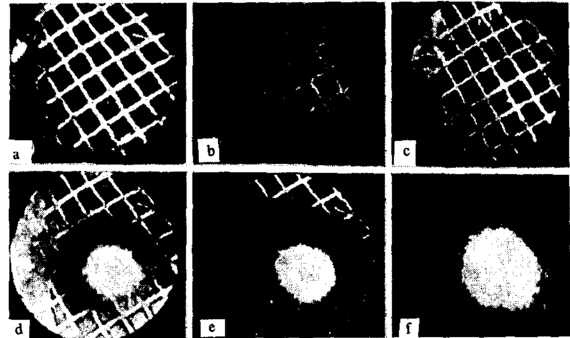

FIG. 18. Electron-mirror images of a lattice with a groove depth of 25 Å for bias voltages [35] in volts of: (a)–8, (b)–0, (c)–0.1, (d)–0.2, (e)–0.6, and (f)–1.

A spread in energy of the illuminating electron beam spoils the resolution: With a tungsten cathode ($kT \approx 0.2$ eV) the realistically achievable δ is approximately 120–150 Å.[77]

The Schrödinger equation for a monokinetic electron beam in a focused MEM has been solved also in Bok's book[13], where the behavior of the potential in a real immersion mirror objective is taken into account. The solution—the first approximation in a series expansion in an arbitrary small parameter—was obtained in the form of Airy functions. It is shown that a sinusoidal perturbation of the potential at the sample surface acts on the electron beam in exactly the same way as a diffraction lattice acts on a light beam with a wavelength equal to the wavelength of the primary monokinetic electron beam. A similar but more rigorous calculation has been made by Hermans and Petterson[98]. However, the resolution of MEM was not calculated in these two studies.

TABLE I

ζ_0	$2\pi a_{\min}$	$\Delta\zeta$	$\Delta x_{\min}$, Å	$\Delta z_{\min}$, Å	U_{bi}, mV	$\lvert\psi_0\rvert^{\max}_{z=0}$, mV
0	3,45	0.70	70	14	0	4
α	4,39	0.19	90	4	14	5
2α	5,75	0.09	120	2	40	7

The resolution of a focused MEM was estimated by Bok et al.[95] on the basis of the Heisenberg relation: for electrons with 30-keV energy the limiting resolution is δ = 8–16 Å. This estimate is extraordinarily optimistic, since the resolution of MEM in the focused mode can hardly exceed by an order of magnitude the resolution of a thermionic emission microscope, which is 140 Å according to the data of Soa.[99]

The limiting resolution of an image with sufficient field of view is strongly limited by the divergence of the primary beam due to the finite size of the source and the effect of the aperture in the anode diaphragm. These geometrical-optics limitations have been discussed in refs. 74 and 100. A quantum-mechanical calculation of the limiting resolution with inclusion of the diverging effect of the anode diaphragm and the geometrical optics of the MEM leads[101] to a dependence of the limiting resolution δ on the instrument parameters different from that obtained by Wiskott: $\delta \sim (l\hbar/p_0)^{1/2}$, while Eq. (35) gives $\delta \sim (l\hbar^2/p_0^2)^{1/3}$ (here $p_0 = (2emU_0)^{1/2}$).

If an MEM is operating in the shadow mode, the image of the sample surface remains sharp for various distances L from the sample to the screen, and therefore instead of the ordinary magnification $M = R_i/r$ (r and R_i are respectively the distances from the axis of the object and image points) we can introduce, following Schwartze[100], the relative magnification V:

$$V = \gamma/r = R_i/r = M/L, \tag{37}$$

where γ is the angle formed by the imaging beam and the axis. Two imaging beams can be resolved if the angle between them is greater than the beam aperture angle $2\alpha_0$. Consequently the minimum resolvable distance between points on the object δ_α, which is limited by the aperture of the imaging beam (the aperture at reflection does not change), is equal to

$$\delta_\alpha = 2\alpha_0/V.$$

Because of the diverging action of the anode diaphragm the electrons acquire an additional radial velocity $\dot{r}_u = dr_u/dt$ at the turning point $z = z_u$ (the designations r_u, z_u, and E_u are from Schwartze's article[100]), and therefore the electron is reflected not over a definite point of the object, but "slips" in the radial direction, and the resolution in this direction deteriorates. Schwartze calculated (by Wiskott's geometrical-optics method) the resolution δ_q limited by this factor for the particular case of reflection of two wave-shaped projections at a distance 2a (the bias voltage was zero):

$$\delta_q = 2a = 0.18 q^2 V^2 r^2 U_0 E_u^{-1}$$

($q = 2\dot{r}_u/\dot{r}$, $\dot{r}$ is the radial velocity of an electron leaving the objective after reflection; U_0 is the accelerating voltage, E_u is the field strength at the sample; it corresponds to Wiscott's E_∞). Thus, the resolution deteriorates in proportion to the square of the distance from the system axis. The resolution in the region near the axis decreases with increasing bias voltage:

$$\delta = 2a \approx 0.4\, z_u = 0.4\, U_{bi}/E_u.$$

As the minimum resolvable distance δ we can take the sum:

$$\delta = \delta_\alpha + \delta_q = (2\alpha_0/V) + 0.18 q^2 r^2 V^2 U_0 E_u^{-1}. \tag{38}$$

An additional limitation is that a sufficient number of resolvable points $N = 2r/\delta(r)$ must be packed into the field of view diameter 2r. The maximum value is

$$N_{max} = 1.67\,(\alpha_0^2 q^2 V U_0 E_u^{-1})^{-1/2}. \tag{39}$$

In this case at the edge of the field of view $\delta = 2\delta_\alpha$.

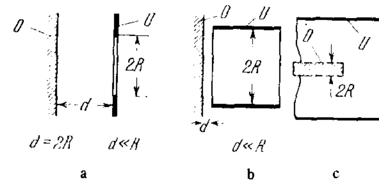

FIG. 19. Various mirror electron-optical systems. [100] a) Lens-diaphragm, b) cylindrical lens, c) object immersed in retarding field.

TABLE II

No. of mirror system	$q = 2\dot{r}_u/\dot{r}$	$\frac{E_u}{U_0}R$	VR	R_0, cm	N_{max}	r, μ	δ, μ
1	0.63	0,49	0.30	0.49	1100	340	0.65
2	0.58	1.00	0.88	1.00	980	420	0.46
3	0.62	1.37	0.96	1.37	1000	300	0.58
4	0.60	0.49	0.49	0.49	890	180	0.40

Schwartze calculated the resolvable distance for three different mirror systems (Fig. 19): sample + diaphragm or cylindrical electrode—the arrangement usually used, and a rod-shaped object placed arbitrarily in a tube (the spherical electron mirror of Artamonov[53,94] is a further development of this design). The results of the calculation are given in Table II. For a comparison of the different systems, we have chosen those values of $R = R_0$ (see Fig. 19) which give identical values of $E_u/U_0 = 1\ \text{cm}^{-1}$. Then, for a given field strength E_u the accelerating voltage U_0 is the same for all systems. The data in Table II are given for an aperture $\alpha_0 = 10^{-5}$. For other values of α, R_0, and E_u/U_0, these data are easily converted by means of Eq. (38) and (39). The parameters given in this table can be used in calculation of the microfield from the image contrast, since it is necessary in the calculation to know the quantities q and E_u (it is usually assumed that approximately $E_u \approx E_0 \approx U_0/l$, where l is the distance from the sample to the anode diaphragm).

As can be seen from Table II, the various mirror systems for $\alpha_0 = 10^{-5}$ and $E_u/U_0 = 1\ \text{cm}^{-1}$ give approximately identical resolution $\delta = 0.5 \pm 0.1$ micron and image quality $N_{max} = 1000 \pm 100$ points in a field of view diameter. A resolution of 500 Å with an aperture $\alpha = 10^{-5}$ can be obtained in such systems if the field strength is raised by an order of magnitude (the geometrical dimensions R_0 are decreased) so that the ratio $E_u/U_0 = 10\ \text{cm}^{-1}$, i.e., if we have, for example, for system No. 1 an accelerating voltage of 10 kV, a field strength E_u = 100 kV/cm, and a diaphragm diameter $2R = d \approx 1$ mm.

Since at the turning point $m\dot{r}_u^2/2 = -eE_u z_u$, reflection occurs at a distance

$$z_u = -(m/2eE_u)(1/4)q^2\dot{r}^2 = -(1/4E_u)q^2(m/2e)\gamma^2\left(-2\frac{e}{m}U_0\right) = (q/4E_u)V^2r^2U_0,$$

and, with a bias voltage U_{bi}, $z_u = (q^2r^2V^2U_0/4E_u) - (U_{bi}/E_u)$ (in analogy with Eq. (17)). For $z_u = 0$, in agreement with Eq. (37), it follows from this that

$$U_{bi} = U_0 q^2 V^2 r^2/4 = U_0 q^2 R_i^2/4L^2; \tag{40}$$

here R_i is the radius of the diffuse secondary emission spot on the screen. This relation can serve to check the

theoretically calculated value of q. Experimental verification of the dependence of the radial resolution on radius (38) has been carried out by Schwartze[100] with use of a transverse magnetic field to displace the region of incidence of the electrons on the sample.[68b] The agreement with theory was satisfactory. With increasing r the image of a point (a sphere of latex) transforms from a star-shaped caustic to a radially located streak, the contrast gradually decreasing.

The radial structure of a shadow mirror image is similar to the pattern produced by an astigmatic, poorly corrected lens of a transmission microscope. In order to avoid this specific geometrical-optics limitation of MEM resolution, Schwartze suggested[100] a use for illumination of a converging electron beam which satisfied the condition $\dot{r}_u = 0$ (q = 0) at the turning point. This idea has been put to use in MEM with focused images.[13,65] Focused images of finely structured grids and other samples obtained in refs. 13, 65, and 102 preserve their sharpness over the entire field of view. However, the sensitivity (i.e., the relative contrast of the images) of MEM in the focused mode is poorer than in the shadow mode[12] for large spatial frequencies $\nu = 10-10^{-3}$ cm^{-1}: demodulation of the beam in the shadow mode of operation (redistribution of the current density) is more efficient than cutting off the deflected electrons by an aperture diaphragm. Furthermore, since the sample in an MEM acts on the beam as a diffraction grating (i.e., as a phase object) and since defocusing leads to an increase of contrast at the expense of resolution,[13] the shadow (projection) mode can be considered as a limiting case of defocusing, focused in magnification.

The influence of the illumination conditions i.e., of the imaging beam parameters, on MEM resolution has also been discussed by Artamonov and Komolov[103a], but mainly for MEM with spherical electrodes, since it was assumed that the image is not formed in an equipotential space. For spherical MEM, whose spectral characteristics have been calculated in detail in refs. 94, 96, and 104, this question is discussed in detail in ref. 103b, where recommendations are given for the choice of optimal conditions of operation with such an instrument, and in ref. 103c, where lens aberrations are taken into account. The limiting resolution of spherical MEM, estimated from geometrical considerations, is 30–80 Å.[103d] The effect of the initial velocity spread on the accuracy of solution of the direct and inverse contrast problems has been taken into account by Nazarov and Sedov[105].

It should be noted that estimates of the limiting resolution and sensitivity obtained by the methods of geometrical electron optics are at best valid only in order of magnitude, since the behavior of the reflected beam in the presence of small perturbations at the sample is correctly described only by means of wave mechanics, as was shown by Wiskott[77] for a periodic perturbing potential by comparison of the reflected-beam current-density distributions calculated by various methods. For this reason the estimates of limiting sensitivity of ordinary MEM (of the order of 0.1 mV) obtained in one of Barnett's articles[106] on the basis of geometrical optics and in addition without inclusion of the tangential velocity spread of the illuminating beam are somewhat in doubt. The usual estimates of the sensitivity are 1–15 mV.[107]

Ordinarily in estimation of the resolution of MEM, the effect of the space charge of the electron beam on the behavior of the reflected electron trajectories is neglected, although for small accelerating voltages and high beam currents the resolution can be limited by just this factor. Artamonov et al.[108] used an analog computer to solve the problem of reflection of the electron beam in a uniform field with inclusion of the effect of space charge (only the radial component of the space-charge field was taken into account). The following formula was obtained for the dependence of the relative beam radius $R = r/r_0$ on the coordinate z:

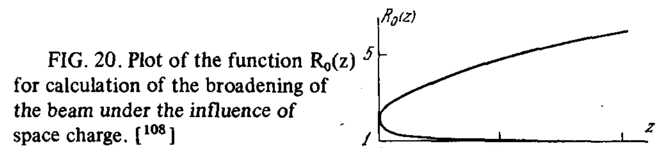

FIG. 20. Plot of the function $R_0(z)$ for calculation of the broadening of the beam under the influence of space charge. [108]

$$R(z, \theta) = 1 + 4.65 \cdot 10^6 (y_0/r_0)^2 P [R_0(z) - 1],$$

where r_0 is the beam radius at the entry into a uniform field whose length is y_0, $z = y/y_0$ is the relative coordinate, $P = I/U^{3/2}$ is the beam perveance, and $R_0(z)$ is the function shown graphically in Fig. 20. If we assume a broadening of the reflected beam (under the action of space charge) at the exit from the uniform field (and, consequently, a deterioration of the resolution) of no more than 10%, we should have $(y_0/r_0)^2 P < 2.5 \times 10^{-8}$ AV$^{-3/2}$. Under the conditions necessary to obtain a resolution of 100 Å, it is necessary[74] to take r_0 = 10 microns and, for y_0 = 0.5 cm and U = 10 keV, the beam current should not exceed I = 0.1 μA; here the image brightness will be low. Therefore the limiting resolution can be achieved only with high accelerating voltages.

7. IMAGING OF MAGNETIC MICROFIELDS

Electron-mirror images of magnetic microfields were first obtained by Spivak et al.[72] By comparison with powder patterns it was shown that the bright portions in the electron-mirror image correspond to places with maximum magnetic field gradient. Mayer[109-113] subsequently continued investigations with MEM of magnetic microfields of various origins—domain structures, fields in sound-recording devices, fields in magnetic tape recording, and artificial samples with an imposed magnetization. He was one of the first to give a qualitative analysis of the problem of magnetic contrast in MEM (the deciphering of this contrast is more complicated than in the electrical case) and to describe certain indications which permit images of magnetic microfields to be distinguished from those of geometrical and electrical relief[109]: 1) the sensitivity of MEM to magnetic fields is increased with removal from the electrical center (the center of the region of incidence of the electrons for positive U_{bi}); 2) if the sample is displaced, the contrast in the image of a magnetic structure changes to the reverse on passing the electrical center; 3) the secondary emission spot is displaced under the influence of a magnetic microfield; 4) radial magnetic structures are imaged with greater contrast than those extended in the azimuthal direction.

The main contribution to the contrast, according to Mayer, is due to the interaction of the radial component of the electron velocity $\dot{r}$ with the magnetic induction component B_z normal to the sample surface, which leads to an aximuthal deflection of the electron $\Delta\varphi$. Here the sample regions over which $\Delta B_z/\Delta\varphi > 0$ will be bright in the image, and the regions with $\Delta B_z/\Delta\varphi < 0$ will be dark.

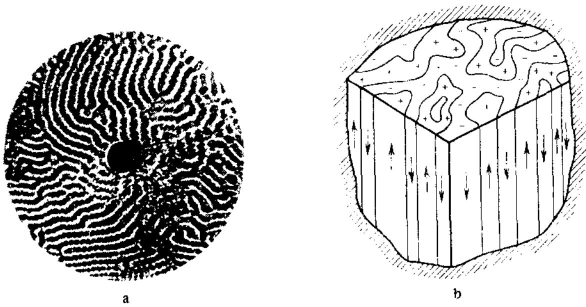

FIG. 21. Electron-mirror image ofthe domain structure of magnetoplumbite (30X) (a) and its interpretation (b).

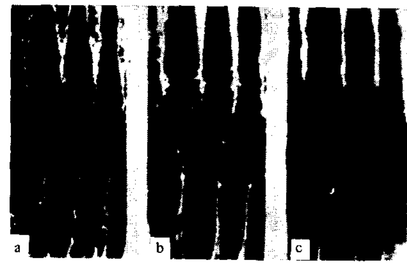

FIG. 22

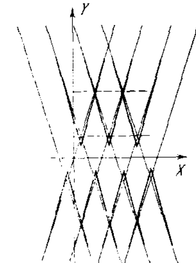

FIG. 23

FIG. 22. Electron-mirror image of domain boundaries in the prismatic plane of a single crystal of cobalt for bias voltages in volts: (a)–0, (b)–6, and (c)–15 (negative bias voltages; 200X; optical center below).

FIG. 23. Caustics in the image of a sinusoidal magnetic field.

As an example of electron-mirror images of complex magnetic structures, we have shown in Fig. 21 the image of the domain structure of magnetoplumbite and a qualitative drawing showing the interpretation of this image, obtained on the basis of this reasoning.[114] Quantitative interpretation of these images is extremely difficult even at the present time.

The first attempt to evaluate quantitatively the contrast of the image of magnetic structures was made by Kranz and Bialas[115]. Assuming, like Mayer, that the contrast is produced only by the component $e\dot{r}B_z$ of the Lorentz force, and with a number of simplifying assumptions, they found the distribution of current density on the screen

$$j(r, \varphi) = j_0 [1 - \text{const} \cdot (\mathbf{j}^{(1)}\mathbf{r} \text{ grad } B_z)], \quad (41)$$

where $\mathbf{j}^{(1)}$ is the current-density unit vector and $\mathbf{r}$ is the polar-coordinate radius vector at the sample. From this equation it follows that the image contrast increases in proportion to r and is maximum if grad $B_z \perp \mathbf{r}$ (i.e., grad $B_z = \partial B_z/\mathbf{r}\partial\varphi$). In addition, on passing the center the contrast changes to the opposite (bright lines become dark), since the sign of the product $\mathbf{j}^{(1)}\mathbf{r}$ grad B_z changes. If B_z = const (grad B_z = 0), there is no contrast and the entire image is rotated by some angle. Thus, Eq. (41) satisfactorily describes almost all the qualitative features of the image of magnetic microfields noted by Mayer.[109] Careful quantitative experimental verification of Eq. (41) has not been carried out.

A unique feature of MEM is that even parallel magnetic domains (for example, domains in the prismatic plane of a cobalt single crystal) are imaged in the form of wedges, there being practically no contrast in a certain band whose center coincides with the optical center of the MEM (Fig. 22). This wedge appearance has been qualitatively explained in refs. 83, 116, and 117 as the result of interaction of the various radial velocity components with the normal component of the magnetic field. Furthermore, in images of domains (see Fig. 22) a bright edge is distinctly visible at the wedge boundaries. This edge corresponds to caustic lines on which a condition similar to Eq. (6) (see section 5) is satisfied. Calculations carried out by Gvozdover and others[118-120] have led to the conclusion that these caustics appear even with a sinusoidal field at the surface ($B_z = B_0 \cos kx$) and in no way correspond to domain boundaries as was previously assumed (see Fig. 23 and compare with Fig. 22a). These caustics are described by equations of the form

$$X = (M/k)\,[2\pi n + \arcsin (M/kAY)] + AY\,[1 - (M/kAY)^2]^{1/2},$$

where X and Y are the coordinates in the plane of the screen, M is the magnification of the microscope, $A = B_0(el\pi/2kmU_0)^{1/2}$, l is the distance from the sample to the anode diaphragm, and n is an integer.

Calculation of the magnetic contrast in MEM for an idealized step-shaped magnetic field has been carried out by Petrov et al.[121] The agreement with the experimental data (the local rotation angle of the image of a ferromagnetic strip with increasing magnetic field was measured and compared with theory) was quite satisfactory.

A more complete calculation of magnetic contrast is given in refs. 122 and 123. The equations of motion are considered for an electron in a retarding electric field $E_0 = U_0/l$ with a magnetic microfield $\mathbf{B}(x, y, z)$:

$$\ddot{x} = \eta_0 (\dot{y}B_z - \dot{z}B_y), \quad \ddot{y} = \eta_0 (\dot{z}B_x - \dot{x}B_z), \quad \ddot{z} = \eta_0 (\dot{x}B_y - \dot{y}B_x) + \eta_0 E_0. \quad (42)$$

The solution is carried out for the condition of a small perturbing microfield

$$|\dot{x}B_y - \dot{y}B_x| \ll E_0.$$

Then, as in the case of electric microfields, the electron motion along the z axis is determined only by the field E_0, and from Eq. (42) it follows (for h = 0) that $\dot{z} = \pm(2\eta_0 E_0 z)^{1/2}$. This gives the possibility of finding, for example, the increase in velocity v_x (similarly for v_y):

$$\Delta v_x = \eta_0 \int (\dot{y}B_z - \dot{z}B_y)\,dt = \left(\frac{\eta_0}{2E_0}\right)^{1/2} \left[-\int_{+\infty}^{0} \frac{(\dot{y}B_z)^{(1)}}{\sqrt{z}}\,dz + \int_{0}^{\infty} \frac{(\dot{y}B_z)^{2}}{\sqrt{z}}\,dz \right] - \eta_0 \left(\int_{\infty}^{0} B_y^{(1)}\,dz + \int_{0}^{\infty} B_y^{(2)}\,dz \right);$$

here the index (1) is for the branch of the trajectory approaching the sample, and (2) for the branch leaving the sample. In the first approximation the last two terms mutually cancel (because of the change of sign of v_z), while the first two terms are equal. If we assume that the displacement of the electron along the x and y axes during its motion in the effectively acting part of the microfield is relatively small (the microfields are sufficiently smooth), we can combine the first two integrals, taking as the integrand function $B_z(x, y, z)$ its value over the imaged point of the sample. This gives

$$\Delta v_x = (2\eta_0/E_0)^{1/2} \int_0^{\infty} \dot{y}B_z z^{-1/2}\,dz.$$

If the y axis passes through the imaged point of the sample, then $\dot{y} = v_r = v_0 r/6l$, where $v_0 = (2\eta_0 U_0)^{1/2}$ is the electron velocity on entry into the uniform retarding field with length l, and U_0 is the accelerating voltage.[74] If we substitute this value of $\dot{y}$ into the equation for Δv_x, and also substitute $B_z(x, y, z)$, expressed in terms of the normal component of the induction at the surface

$B_{0z}(x, y)$, as the solution of the Neumann problem (the equation is identical to (13) but instead of ψ and φ, B_z and B_{0z} are used, respectively), it is possible[122] to obtain an equation similar to (14) where instead of $\Delta\mathbf{v}$ we will have Δv_φ (the increment in azimuthal velocity) and instead of grad φ we will have B_{0z}.

We then find the azimuthal displacement of the electron $\Delta S = (\Delta v_\varphi/v_0)L$ during traversal of the distance L from the anode diaphragm to the screen, and the rotation angle of the image on the screen arising as a result of this displacement: $\gamma = \Delta S/R = \Delta v_\varphi L/v_0 R = 2l\Delta v_\varphi/rv_0$, where R is the distance from the axis to the point on the screen at which the electron hits ($R = Mr = Lr/2l$; M is the magnification). It is necessary also to take into account the additional angle of rotation of the image arising in passage of the electrons, after leaving the region of action of the perturbing microfield, up to the diagram. This angle, as it turns out, is equal to the angle developed in passage of the electrons from the anode diaphragm to the screen.[124] Finally, for the one-dimensional distribution of the field at the surface we obtain

$$\gamma = (\eta_0/2E_0)^{1/2}\int_{-\infty}^{\infty} B_{0z}(x-\xi)\,[h^2+(h^2+\xi^2)^{1/2}]^{1/2}(h^2+\xi^2)^{-1/2}\,d\xi; \quad (43)$$

here γ is the local aximuthal angle of rotation of the image on the screen of an MEM with a two-electrode immersion objective, $B_{0z}(x)$ is the distribution of the normal component of the magnetic field at the sample surface, $E_0 = U_0/l$ is the intensity of the uniform retarding field at the sample surface, and h is the height of reflection of the electrons above the surface. The three-dimensional problem is solved in a similar manner[122] (for a two-dimensional distribution of the field on the surface).

The contrast of magnetic-microfield images (i.e., the current-density distribution at the screen), as in the electrical case, is calculated assuming conservation of tubes of current according to Eqs. (18)—(20), where $S(X) = \gamma(X)R$ is the azimuthal displacement of the electron (one-dimensional field at the surface). If we introduce at the screen rectangular coordinates $X = R\cos\varphi$, $Y = R\sin\varphi$, the displacements in the coordinates X and Y will be expressed in terms of the displacements ΔR along the radius and ΔS in azimuth as follows:

$$\Delta X = (X\Delta R - Y\Delta S)/R,\ \Delta Y = (X\Delta S + Y\Delta R)/R. \quad (44)$$

For two-dimensional microfields on the surface the calculation of contrast must be carried out with the equations[84]

$$j(X'; Y') = j_0(X; Y)\left[D\left(\frac{X'; Y'}{X; Y}\right)\right]^{-1} \approx j_0(X; Y)\left[1-\frac{\partial\Delta X}{\partial X}-\frac{\partial\Delta Y}{\partial Y}\right],$$
$$X' = X+\Delta X,\ Y' = Y+\Delta Y. \quad (45)$$

Equation (43) for the local angle of rotation of the image is an integral equation with respect to the function $B_{0z}(x)$. If this equation is solved by the method of Fourier transforms, we can find[122] the desired magnetic field at the surface (h = 0) for a known local angle of image rotation:

$$B_{0z}(x) = (1/4\pi)(2E_0/\eta_0)^{1/2}\int_{-\infty}^{\infty}[\gamma(x)-\gamma(x-\xi)]\,|\xi|^{-3/2}\,d\xi. \quad (46)$$

The function $\gamma(x)$ can be determined experimentally from the magnitude of the image displacement at individual points on turning on the perturbing field, i.e., by comparison of two images on the screen: in the presence and in the absence of the microfield. It is also possible

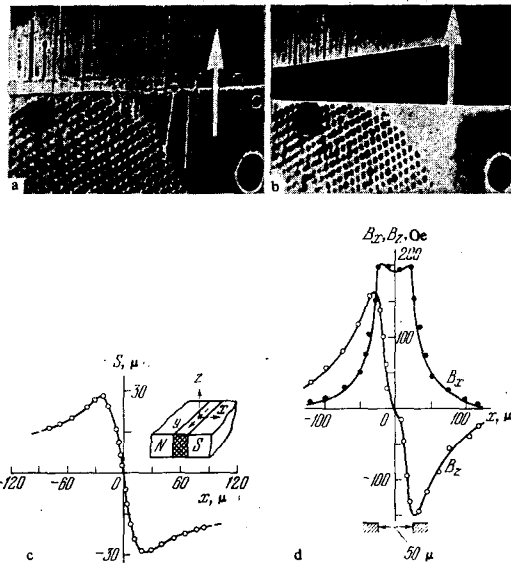

FIG. 24. Calculation of electron-mirror images of the magnetic-mirror images of the magnetic-field distribution over the gap of a magnetic head. a) Image of surface of head with working gap and deposited scale grid (period 30 microns) without coil current; b)—with current in head coil (the arrows in parts a and b denote the image scanning line; the dark spot at the bottom right is the image of a hydrocarbon film); c) displacement of trajectories as a function of the coordinate, obtained from an oscillogram; d) distributions of the normal component B_z and tangential component B_x of the field, calculated by computer according to Eqs. (46) and (47).

to find $\gamma(x)$ from the image contrast if we use the same procedures as for electric microfields (see Eq. (21) and Fig. 14).

As an illustration of the latter method we have shown in Fig. 24 all of the steps in obtaining the magnetic field distribution above the gap of a magnetic head: electron-mirror microphotographs of the surface of the head with the working gap (a scale grid has been deposited on the surface) with the coil current turned off and turned on (in the latter case the characteristic dark wedge appears in the image); the azimuthal displacements of the electrons calculated from oscillograms of the current-density distribution (curve S(x)) and distributions of the normal and tangential components of the field above the working gap calculated by computer. The tangential component B_{0x} was calculated with the equation:

$$B_{0x} = (1/\pi)\int_{-\infty}^{\infty} B_{0z}(\xi)\,(x-\xi)^{-1}\,d\xi. \quad (47)$$

The equations given above were obtained for MEM with a two-electrode objective and on the assumption of small deflections of the electron during its passage through the microfield. For a three-electrode objective similar equations have been obtained by Gvozdover,[118] who calculated the contribution to the image contrast not only of the normal component of the field but also of the gradients of the tangential components. This contribution turns out to be of the same order as the contribution of the normal components.[125]

The formation of magnetic contrast in MEM is described mainly by the equations given above, which were obtained in *first-order perturbation theory*. However, in many cases it is necessary to take into account in addition a number of second-order effects.[122] For example, interaction of the normal component of the electron

velocity v_z with the tangential components of the microfield B_x and B_y as the result of the change in sign of the velocity v_z in the electron's approach to the sample and travel away from it leads only to a displacement of the electron trajectory and in the first approximation (taking into account the change in the slope angle of the trajectory) drops out. However, it must be noted that as a result of this interaction of v_z and, for example, B_x the electrons acquire in the lower part of their trajectory an additional tangential velocity Δv_y, whose appearance in turn produces an effect which, though secondary, is important. Specifically, the appearance of the additional tangential velocity Δv_y and its interaction with the normal component of the microfield B_z leads to appearance of an additional velocity along the other tangential coordinate (the x axis). Consideration of the direction of this additional secondary velocity shows that it always leads to a displacement of the electron in the direction of increase of the absolute value of the microfield intensity. For example, in the case of reflection by a ferromagnetic strip magnetized normal to the sample surface, this additional velocity is directed toward the center of the strip and therefore results in a narrowing of the image of the strip on the screen.

The appearance of Δv_y produces also a shift above the sample surface of the point where the tangential component of the electron velocity is zero. This point is revealed by the appearance of a secondary-emission spot when a positive bias relative to the electron gun cathode is applied to the sample. Thus, the secondary-emission spot on the sample is displaced. In imaging of a ferromagnetic strip the displacement Δy of the secondary-emission spot occurs along the strip. The direction of the displacement of the spot is opposite to the direction of the additional tangential velocity Δv_y, since the secondary-emission spot is formed at the place where the combined tangential velocity of the electron is zero, i.e., where the additional tangential velocity and the initial radial component of the electron velocity v_r compensate each other: $\Delta v_y + v_r = 0$. The displacement of the secondary-emission spot has been calculated by Sedov et al.[122] and can be used for calculation of the magnetic microfields which produce this displacement.

Equations (43)—(45) for the magnetic contrast have been experimentally verified for a sample with a known field distribution—a wire with a current,[126,127] heating of the wire being avoided by pulsing the current and operating the MEM in a stroboscopic mode.[128] The test showed rather good agreement of the theoretical and experimental results (a discrepancy of no more than 20%), which is not the case with the result of Kranz and Bialas, Eq. (41).

Comparison of results obtained by MEM and in a magneto-optical apparatus also showed completely satisfactory agreement of the results of the two independent methods of measuring the magnetic fields.[129a]

8. APPLICATIONS OF MEM IN PHYSICS RESEARCH

a) Studies of contact fields and semiconductors. The first work on contact fields was done by Orthuber[33] who observed patch fields—contact fields between a nickel substrate and layers of Ba or BaO. He also constructed the first image converter: an optical image PbS; the relief was read by means of an MEM. A similar converter based on Se-Bi has been described by Bates.[130] Study of patch fields of various natures by means of MEM has been carried out by Spivak et al.[32,131] In particular, patch fields in secondary emitters and the effect of these fields on the velocity distribution of the secondary electrons have been studied over a wide temperature range; oxide and L cathodes were studied. Electron-mirror images were compared with thermionic and photo-electric emission images. Use of a combined emission-mirror microscope provides the possibility of quantitatively evaluating the distribution of the work function over the surface of a patch emitter.[132a] The possibilities of MEM are briefly discussed by Newberry.[132b]

A number of investigations by Igras and Warminski[45,133-137] and other authors are devoted to contact fields in semiconductors: MEM were used to observe p-n junction fields,[133,138] dislocations in silicon,[134] contact fields of oxides on semiconductor surfaces, the impurity surface-diffusion front (diffusion of lithium in silicon),[135] and various inclusions and contaminations; the drift of lithium ions was studied along radiation defects in silicon obtained as the result of irradiation of silicon by a beam of 1-MeV electrons[137]; images were obtained of integrated circuits[136] not covered by silicon oxide films. Dielectric nonuniformities of films[139] and band structures[140] have been observed. In these studies, however, the MEM was used mainly as a device intended for visualization of contact fields of various types.

Although the first electron-optical images of p-n junction fields were obtained in an MEM,[141] electron-mirror methods of measuring these fields have been developed only comparatively recently. The first attempt to make such measurements was the work of Sedov et al.[142], who described a method of measuring the potential distribution on the surface of a semiconductor diode with a p-n junction from the displacement of the secondary-emission spot. The idea of this method is simple: the positive voltage on the sample is varied (for a fixed reverse voltage on the diode), and the displacement is recorded of the edge of the secondary-emission spot arising at those parts of the surface hit by the electron beam. A spot appears only at those places whose potential is greater than or approximately equal to the electron-gun cathode potential, and the boundary of the spot is an equipotential line whose potential is equal to the cathode potential of the gun (within the contact-potential difference, if the energy spread in the illuminating beam is not taken into account). Therefore, for a fixed reverse voltage on the diode it is possible to find the potential distribution on the surface if the displacement of the spot boundary is measured as the bias voltages changes.

The accuracy and localization indicated by these authors for this method of measurement (0.1 μ and 0.1 V) are exaggerated, since the spot boundary is quite diffuse as the result of the spread in velocity and divergence of the illuminating beam; in addition, it is necessary to make a correction for the tangential velocity component and the corresponding decrease in the normal component on passage of the electrons into the region of the microfield (the displacement of the primary beam and the resulting redistribution of current density have been calculated in ref. 143). However, the measured results can be distorted substantially as the result of appearance of

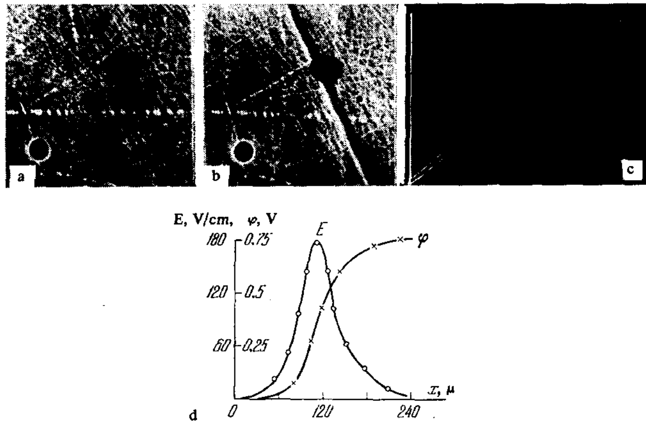

FIG. 25. Electron-mirror microphotographs (a, b), integral curves of signal image (c), and distributions of field and potential calculated from them over the surface of a GaSb diode. a) Reverse voltage not applied; b) reverse voltage 0.75 V, bias voltage 5V (h = 1.5 μ; the dark spot at lower left is the image of a hydrocarbon film, and that at upper right is an opening in the screen); c) integral curves for bias voltage of 50 V (h = 15 μ) and reverse voltage 0 and 0.75 V; d) distribution of field E and potential ϕ at a height h = 15 μ above the diode surface.

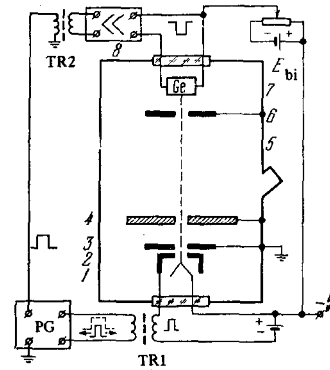

FIG. 26. Block diagram of stroboscopic MEM. 1-3—Electron-gun electrodes, 4—luminescent screen, 5—window for observations, 6—anode diaphragm, 7—sample studied, 8—amplifier-shaper; PG—pulse generator TR_1, TR_2—isolation transformers, E_{bi}—bias battery.

contaminating hydrocarbon films, which are polymerized and intensely charged by the electron or ion beam. The ion beam bomarding the sample arises as the result of ionization by the electron beam of the residual gas in the instrument, and for a vacuum of the order of 10^{-4} mm Hg, according to estimates by Schwartze,[144] the ion current density amounts to about 1/20 of the electron current density.

Mention should be made of the very high sensitivity of MEM to surface impurities on the sample, particularly to poorly conducting films which are charged by fast electrons from the tail of the Maxwellian distribution or by ions. Charging of dielectric and semiconducting films by the electron beam leads to appearance in the electron-mirror photographs of characteristic dark spots with a white edge (see, for example, Fig. 24a or 25a) which are images of negatively charged islands of the film. At some distance from the electrical center, where the ion current to the sample exceeds the current produced by fast electrons, hydrocarbon or other films are charged positively and white star-shaped caustics appear in the image.[144,145] The calculated shape of the caustic surfaces arising on reflection of electrons in a field of even a point positive or negative dipole (a charge of the opposite sign is induced in the substrate, so that a dipole is usually formed) corresponds to the images obtained.[146]

On the one hand, the MEM provides the possibility of estimating the conductivity of surface films[145,147,149] and following polymerization processes resulting from electron or ion bombardment.[145,148-150] On the other hand, the increased sensitivity of MEM to surface impurities, which is not present in most types of emission and scanning microscopes, complicates the visualization and measurement of electric and magnetic microfields: it is necessary to prepare the samples carefully and to freeze out hydrocarbon impurities, which appear mainly at the points of maximum gradient of the microfields—at the cleavage steps,[145] in the vicinity of the p-n junction in a semiconductor diode,[151] and so forth. This peculiar decoration of the surface being studied, together with the charging of local dielectric films, often greatly hinders the quantitative interpretation of electron-mirror images, which are sometimes completely covered by dark spots with white edges, as for example, in one of the interesting studies devoted to the charging of film microcircuits.[152] Such contamination can apparently be completely avoided only in an ultrahigh vacuum microscope with oil-free pumps.

In the case of sufficiently smooth surfaces and in the absence of bombardment of the surface being studied by an electron beam (negative bias voltages), hydrocarbon impurities do not distort the images too strongly and the field distribution on the sample surface can be calculated from the electron-mirror image by the method described above (see section 5, Eq. (22)), i.e., calculating by computer the field and potential at the surface from oscillograms of the current-density distribution at the screen. This means has been used[84,127,147,153] to measure the fields of p-n junctions and metal film structures. As an illustration of this method we have shown in Fig. 25 the fields measured above a semiconductor diode (the field can be measured at practically any height above the sample). This method has been used in a simplified version[154] to measure the field of the p-n junction. In many cases it is possible to measure the potential with an accuracy of about 0.1 V and the localization to better than 1 micron.

Stroboscopic MEM (Fig. 26) have been used to study the switching of silicon and germanium diodes from the cut-off state to the conducting state.[155] The voltage pulses fed to the diode were synchronized with the stroboscopic pulses triggering a normally biased-off electron gun of an MEM. If the stroboscopic pulses are shifted in phase with respect to the pulses fed to the sample, it is possible to fix any stage of the switching process (or of any periodic process).

Stroboscopic MEM have been used very effectively to observe recombination waves in germanium.[156] In this work the authors obtained an image of the active region in which the maximum electric field appears on application of a voltage pulse to the germanium sample, and it was established that the active region is formed in a limited portion of the samples and is located closer to the more negative electrode. The method of Sedov et al.[84] was used to calculate distribution curves for the field strength and potential along the sample surface. The results obtained were compared with measurements made with a clamped probe, and both qualitative and quantitative correspondence was observed between the

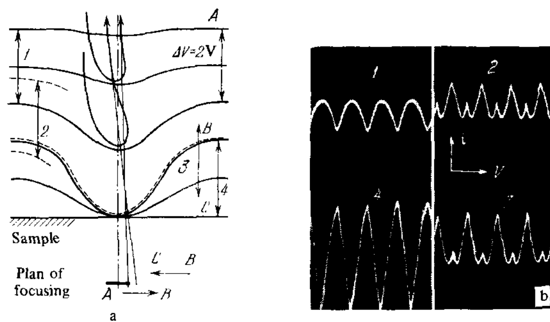

FIG. 27. Deflection and modulation of reflected beam as the result of induced charge. a) Equipotentials and electron trajectory; b) oscillograms of i(V) for various reflection zones. [159]

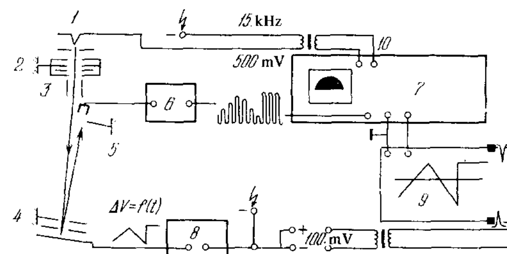

FIG. 28. Plot diagram of microscope-voltmeter [159] 1—Electron-gun cathode, 2—electrostatic condenser, 3—deflecting plates, 4—mirror objective, 5—screen for observation and Faraday cup (on the axis of the mirror objective), 6—preamplifier, 7—amplifier with synchronous detector, 8—generator of sawtooth bias voltage supplied to sample, 9—recording device, 10—high frequency output modulating the beam.

results obtained by the two independent methods. It should be noted that the observations and measurements were made with a very low duty cycle of the stroboscopic pulses (the ratio of the duration to the period)—one part in from 2000 to 4000, i.e., with a very low current density at the screen. Stroboscopic MEM for observation of piezoelectric fields with frequencies up to 100 MHz have been described by Szentesi and Ash.[157]

An interesting method for investigation of semiconductor and film structures has been developed in France by Guittard and co-workers.[158,159] This method is based on detection of the comparatively small defocusing and deflection of the reflected beam by the field of induced charges arising on the sample surface as the electrons approach it (Fig. 27). A sample at a small negative bias voltage relative to the electron cathode is fed a symmetric saw-tooth voltage V with a period of the order of 100 seconds (Fig. 28). A Faraday cup is placed in the center of the screen for observation of the final image. The current i is amplified and detected by a synchronous detector. The dependence of the current i on the bias voltage has a characteristic minimum corresponding to maximum deflection of the reflected beam by the field of the induced charges (the subsequent maximum is due to collision of the electrons with the sample surface; see the series of oscillograms for various reflection zones with a saw-tooth amplitude of 2 V in Fig. 27b). The minimum occurs at different bias voltages for samples of different composition, which permits the contact potential difference to be determined.

It has also been established experimentally that there is a linear dependence of the height of the current peaks on the potential of the surface as the latter is varied in a region of the order of 100 mV. This provides the possibility of determining the surface potential with an accuracy to 0.1 mV if the measurements are made from the current maxima arising when the beam hits the surface, or with an accuracy of 1 mV in the total reflection mode. In spite of the exceptional sensitivity, this method has not yet been used in other laboratories, evidently because of the poor geometrical resolution (no better than 10 microns) and very high requirements on surface purity, since in an ordinary vacuum with multiple collisions of the electron beam with the surface the characteristic current minimum is displaced and then disappears as the result of charging of polymer and oxide films arising on the sample. In the latest ultrahigh vacuum models of microscope-voltmeters[160-162] with a vacuum of $10^{-8}-10^{-11}$ mm Hg, very high stability of measurements have been achieved,[160] and the range of

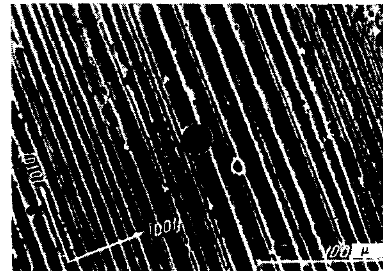

FIG. 29. Electron-mirror image of domain structure of barium titanate.

measurable potentials has reached 4 V with an accuracy of 5 mV,[160] but the geometrical resolution has not yet been improved. Images of microcircuits have been obtained and the potential of a zone with phosphorus ions implanted in the silicon has been measured.[161] The authors do not present a detailed theoretical discussion of the technique developed.

b) Studies of dielectrics. Ideal insulators cannot be studied in ordinary MEM, since the sample surface is rapidly charged by the electron beam. Therefore massive samples with resistivity $\gtrsim 10^8$ ohm-cm are usually covered beforehand with a thin film of metal or semiconductor with a surface conductivity sufficient for removal of the charge, although in particular situations it is possible to stabilize the surface potential of a dielectric being studied by equalizing the electron and ion currents to the sample, i.e., by appropriate choice of the bias voltage.[163]

MEM have been used to study the domain structure of various ferroelectric materials—barium titanate[38,39,164,165] (Fig. 29), triglycine sulfate,[163] lead zirconate-titanate,[130] $Ca_2Sr(C_2H_5CO_2)_6$,[167,168] and other compounds[165,166] over a wide temperature range. Observations have been made of the transition from the ferroelectric phase to the paraelectric phase on passing through the Curie point, repolarization on application of an external field,[164] nucleation of domains in the process of crystal growth of a lead zirconate-titanate crystal,[164] and visualization of 180° domains, whose images cannot be obtained in a polarization microscope.[165,168] Specific studies have been made of the topography of a surface on which geometrical relief appears in the transition of barium titanate to the ferroelectric phase, and the electric microfields of domains (in order to obtain a picture of only the geometrical relief, the sample was covered by a gold film about 500 Å thick) in barium titanate.[164,165,168] Someya et al.[169]

estimated the size of the geometrical irregularities on the surface of barium titanate in the ferroelectric phase by means of Eq. (23), solving the problem of electric-microfield image contrast with the approach set forth above in section 5.

MEM have been used not only for image converters,[33,130,149] but also as electron-acoustic converters, i.e., for visualization of piezoelectric waves on the surface of quartz plates. In Koch's converter[170] the sample, in a cell with water, was irradiated with an ultrasonic wave and the transmitted signal excited a piece of quartz mounted as a sample-reflector in an MEM. Electron-mirror images of the sample obtained by these means were extremely blurry, particularly since the picture of the surface piezoelectric wave obtained was not instantaneous but averaged over time.

For observation and measurement of the distribution of a piezoelectric field at various moments of time, stroboscopic MEM[171] have been used. It has been shown[118,171-173] that in the ordinary mode of operation of MEM it is impossible to obtain an image of a traveling wave, and the image of a standing wave has a factor of two shorter period and weaker contrast than the image in the stroboscopic mode. Equations have been obtained which describe the contrast of traveling-wave and standing-wave images in the various modes of operation of MEM. For the particular case of a standing wave produced by two opposing traveling sine waves with a wave vector $k = 2\pi/\lambda$ and angular frequency ω, for example, the relative contrast of the electron-mirror image in the stroboscopic mode (to first order) is

$$K(x';\ t') = (j - j_0)/j_0 \approx kA_0 \cos \omega t' \cdot \cos kx',$$
$$x' = x - A_0 \sin kx \cdot \cos \omega t',$$

where $A_0 = 6\varphi_0(\pi k l/E_0^2)^{1/2}\exp(-kz_0)$, φ_0 is the amplitude of the potential, z_0 is the electron reflection height, and $\omega t'$ is the observed phase of the process. In the ordinary mode the relative contrast is

$$K(x') \approx (k^2A_0^2/2)\cos 2kx',$$

i.e., the pattern is repeated with a double frequency and its contrast is smaller by a factor $2/kA_0$. With increase of the amplitude of the potential or decrease of the strength of the retarding uniform field, the contrast increases and caustics appear in the image. The contrast has also been calculated for two-dimensional piezoelectric fields.[174]

Pictures have been obtained of volume and surface (Rayleigh) waves in quartz, quartz bombarded with protons,[175] lithium niobate, and cadmium sulfide, the amplitudes of the field strength and potential of the piezoelectric fields at various heights above the sample surface[173,175] being calculated by the method described above in section 5 for solution of the inverse problem.

MEM have been used also for the study of biological objects.[176] The sample—chloroplast obtained from sectioning of single-cell marine algae—was covered with a thin layer of copper (resistivity from 10^3 to 10^6 ohms/square). Observations were made both of the surface topography of the sample and of charged centers which appeared distinctly with a rapid increase of the negative bias voltage between the gun cathode and the sample. McLeod and Oman[176] discuss the relation between these centers and the reactive centers which transform electromagnetic energy into chemical energy. For a definitive solution of this problem it is necessary first of all to avoid completely the appearance on the sample of hydrocarbon impurity films which can behave in a similar way with change of bias voltage.[145]

MEM are used also for investigation of thin dielectric layers and structures of the metal-dielectric and metal-dielectric-metal type.[152,153,177]

c) Visualization and measurement of magnetic microfields. A large number of studies have been made of the visualization and measurement of magnetic microfields by means of MEM. After the appearance of refs. 41, 72, 76a, 83, 116 and the work of Mayer[110-113], who demonstrated the possibility of obtaining images of magnetic fields with MEM and made the first attempts at quantitative evaluation of these fields, a first-approximation theory of the contrast of magnetic-field images in MEM was developed, and MEM are used at the present time not only as microscope-voltmeters but also as gaussmeters.

The domain structure of various ferromagnetic materials has been studied visually in refs. 39, 83, 100–113, 114, 138a, and 178. Spivak et al.[179] and Ivanov[180] attempted to measure the magnetic-field distribution inside domain boundaries, but the resolution of the MEM used was insufficient and there was as yet no theoretical basis for calculation of the field from the images.

Many workers have studied the fields of magnetic heads of various types.[110-113,116,122,129a] here Sedov et al.[122] and Rau et al.[129a] used the method described above for solution of the inverse problem of the contrast of magnetic-microfield images, which provided the possibility of measuring the distribution of the magnetic field above the gap of the head.

The stroboscopic method of studying variable magnetic fields by means of MEM, which has been described by Spivak and Luk'yanov[181], has provided the possibility of measuring the frequency and phase characteristics of magnetic heads, i.e., the dependence of the amplitude and phase of the magnetic field above the gap of the head on the frequency for a fixed current amplitude in the exciting winding. The essence of the method is that when either a sinusoidal or direct current is supplied to the exciting winding of the magnetic head, it is frequently possible (if the field configuration over the gap does not change with frequency) to select an equivalent direct current which produces the same constant field over the gap as an alternating current of fixed amplitude and given frequency. Here the electron-optical image of the magnetic field and oscillograms of the brightness distribution on the screen coincide. If we take the ratio of the equivalent constant current I to the fixed value of alternating current amplitude I_0 and leave the stroboscopic pulse phase unchanged, it is possible to determine the relative intensity of the magnetic field above the gap of the head over a wide range of frequencies—from 0 to 10 MHz.

Measurements have also been made[129] of magnetic fields of signals recorded on magnetic tape. Spivak et al.[182] have measured the fields of video heads and video tape signals up to frequencies of 5 MHz and recording wavelength of 8 microns. To increase the contrast in the images of the magnetic fields of signals, Guittard et al.[183] suggests decentering the illuminating beam in a direction perpendicular to the direction of

magnetic induction. Here the tangential velocity component of the electrons and the Lorentz force which produces the magnetic contrast are increased, but the resolution deteriorates. Guittard et al. proposed construction of a device for reading pulse signals recorded with high density on sound-recording tape. Reading can be accomplished without placing the film in vacuum—through a thin (about 5 micron) metallized mica diaphragm. A similar idea for reading electric microfields through a vacuum-tight semiconductor film has been suggested by Weissenberg[184]. The results of practical use of these ideas have not yet been published.

In addition to the ordinary applications of MEM which have already been discussed, this instrument has been used for observation and study of the structure of frozen magnetic fluxes in superconductors.[185] It is possible to study not only thin films[186] but also massive samples of superconducting materials (Pb, Nb_3Sn, and so forth), and to evaluate the structure and the magnitude of the residual magnetic flux.

A number of applications of MEM for study of magnetic microfields of various natures have been discussed in the review by Petrov et al.[187]

Thus, mirror electron optics and microscopy are being perfected, are finding various fields of application, and permit contact-free measurement of microfields to be accomplished.

[1] G. V. Spivak, G. V. Saparin, and M. V. Bykov, Usp. Fiz. Nauk 99, 635 (1969) [Sov. Phys.-Uspekhi 12, 756 (1970)].
[2] P. R. Thornton, Scanning Electron Microscopy, Chapman and Hall, 1968.
[3] G. Möllenstedt and F. Lenz, Adv. Electron. and Electron Phys. 18, 251 (1963).
[4] Yu. M. Kushnir, D. V. Fetisov, L. B. Rozenfel'd, and A. M. Rozenfel'd, Zavod. lab. (Industrial Laboratory) 27, 1528 (1961).
[5] V. M. Kel'man and S. Ya. Yavor, Élektronnaya optika (Electron Optics), 3rd ed., Leningrad, Nauka, 1968, p. 474.
[6] A. Delong and V. Drahos, Proc. of the 3rd European Regional Conf. on Electron Microscopy, vol. A., Prague, 1964, p. 25.
[7] R. D. Ivanov and M. G. Abalmazova, Izv. AN SSSR, ser. fiz. 30, 784 (1966) [Bull. USSR Acad. Sci., Phys. Ser., p. 813].
[8] W. C. Nixon, R. V. Ely, and C. R. E. Legg, Electron Microscopy (Proc. of the 5th Intern. Congress on Electron Microscopy, Philadelphia, 1962), v. 1, N.Y.—London, Academic Press, 1962, D1.
[9] R. Buchanan and W. C. Nixon, in ref. 6, p. 119.
[10] V. N. Vertsner and Yu. V. Chentsov, Izv. AN SSSR, ser. fiz. 24, 519 (1959) [Bull. USSR Acad. Sci., Phys. Ser.]; Prib. Tekh. Eksp. No. 5, 180 (1963) Instrum. Exp. Tech.
[11] L. Mayer, Electron Mirror Microscopy, The Encyclopedia of Microscopy, ed. by G. L. Clark, N. Y., Reinhold—London, Chapman, 1961, p. 316.
[12] R. M. Oman, Adv. Electron. and Electron Phys. 26, 217 (1969).
[13] A. B. Bok, A Mirror Electron Microscope, Delft, Hooglanden Waltmann, 1968.
[14] a) A. B. Bok, J. B. LePoole, J. Roos, and H. de Lang, Adv. Opt. and Electron Micr. 4, 161 (1971); b) Electron Mirror Microscope JEM-M1, JEOL News 6M (1), 2 (1968).
[15] H. Bethge and J. Heydenreich, a) Adv. Opt. and Electron Micr. 4, 237 (1971); b) Exper. Techn. Phys. 19, 375 (1971).
[16] Patent No. R-121694, Physics Institute, Polish Academy of Sciences—the ZME-2 microscope (product of the Polish Optical Plant PZO, Warsaw).
[17] Yu. V. Vorob'ev, Izv. AN SSSR, ser. fiz. 23, 694 (1959) [Bulletin USSR Acad. Sci., Phys. Ser.].
[18] G. Möllenstedt and H. Gruner, Optik 27, 602 (1968).
[19] R. Castaing and L. Henry, C. R. Acad. Sci. 255, 76 (1962).
[20] R. Castaing and L. Henry, J. Micr. 3, 133 (1964).
[21] R. Castaing, A. El. Hili, and L. Henry, C. R. Acad. Sci. 261, 3999 (1965).
[22] L. Henry, Bull. Soc. Franc. Minéral. et Cristallogr. 88, 172 (1965).
[23] R. Castaing, A. El. Hili, and L. Henry, Optique des Rayons X et Microanalyse, P., Hermann, 1965, p. 77; A. El. Hili, J. Micr. 5, 669 (1966).
[24] M. Baril, Can. J. Phys. 48, 2487 (1970).
[25] G. Slodzian, Ann. de Phys. 9, 591 (1964).
[26] W. Schaffernicht et al., FIAT Rev. German Sci., pt. 1, 2, 100 (1948).
[27] M. Auphan, Infrared Phys. 3, 77 (1963).
[28] V. Jareš, Slaboproudy obzor 22, 19 (1965); 3rd Czech. Conference on Electronics and Vacuum Physics. Transactions, Prague, 1967, p. 589.
[29] A. Rusterholtz, Electron Optics (Russ. transl.) Moscow, IL, 1952.
[30] G. Hottenroth, Ann. d. Phys. 30, 689 (1937).
[31] A. Illenberger, Microscopie 19, 316 (1964).
[32] G. V. Spivak, I. A. Pryamkova, and N. N. Sedov, Izv. AN SSSR, ser. fiz. 24, 640 (1960) [Bull. USSR Acad. Sci., Phys. Ser.].
[33] R. Orthuber, Z. Angew. Phys. 1, 78 (1948).
[34] G. Bartz, G. Weissenberg, and D. Wiskott, Radex-Rundschau, Hf. 4/5, 163 (1956).
[35] G. Bartz, G. Weissenberg, and D. Wiskott, Proc. of the 3rd Intern. Conference on Electron Microscopy (London, 1954), L. 1956, p. 395.
[36] L. Mayer, J. Appl. Phys. 26, 1228 (1955).
[37] A. Septier, Ann. Radioelectr. Compagne Franc. Assoc. TSF 9, 1 (1954).
[38] G. V. Spivak, E. Igras, I. A. Pryamkova, and I. S. Zheludev, Kristallografiya 4, 123 (1959) [Sov. Phys.-Crystallogr. 4, 115 (1959)].
[39] G. V. Spivak, I. A. Pryamkova, and E. Igras, Izv. AN SSSR, ser. fiz. 23, 729 (1959)
[40] G. V. Spivak, A. E. Luk'yanov, S. D. Toshev, and V. A. Koptsik, ibid. 27, 1199 (1963) [Bull. USSR Acad. Sci., Phys. Ser., p. 1177].
[41] I. A. Meshcheryakova, Pryamkova, Candidate's dissertation, Moscow State University, 1961.
[42] a) G. V. Spivak, I. A. Pryamkova, D. V. Fetisov, A. N. Kabanov, L. V. Lazareva, and A. I. Shilina, Izv. Akad. Nauk, SSSR, ser. fiz. 25, 683 (1961) [Bull. Acad. Sci. USSR, Phys. ser.]; b) G. Bacquet and A. Santouil, C. R. Acad. Sci. 255, 1263 (1962).
[43] J. Heydenreich, Wiss. Zs. Pädagog. Hochschule Potsdam, 6, 25 (1960).
[44] a) H. Bethge, J. Hellgardt, and J. Heydenreich, Exper. Techn. Phys. 8 (2), 49 (1960); b) O. I. Szentesi, J. Phys. E4, 1076 (1971).
[45] E. Igras and T. Warminski, Phys. Stat. Sol. 9, 79 (1965).
[46] M. E. Barnett and W. C. Nixon, J. Sci. Instr. 44, 893 (1967).
[47] T. Someya and M. Watanabe, Proc. of the 4th European

Regional Conference on Electron Microscopy, v. 1, Rome, 1968, p. 97.
[48] G. Becherer, H. J. Fitting, and F. Kuhlmann, Exper. Techn. Phys. 18, 385 (1970); G. Becherer and F. Kuhlmann, ibid. 19, 119 (1971).
[49] L. Mayer, R. Rickett, and H. Stenemann, in ref. 8, D10.
[50] W. Schwartze, Exper. Techn. Phys. 14, 293 (1966).
[51] L. Mayer, U. S. Patent, Cl. 3.047.719, 31 July 1962.
[52] R. M. Oman, Proc. of the 2nd Intern. Conference on Electron and Ion Beam Science and Technology, v. 1, N.Y., 1966, p. 89.
[53] O. M. Artamonov, in ref. 47, p. 99.
[54] J. Heydenreich, Microscopie Electronique—1970 (Proc. of the 7th Intern. Conference on Electron Microscopy), v. 2, p., 1970, p. 31.
[55] G. Turner and B. Bauer, Proc. of the 6th Intern. Congress on Electron Microscopy, v. 1, Kyoto, 1966, p. 163.
[56] Chuan C. Chang, Rev. Sci. Instr. 42, 189 (1971).
[57] E. Kasper and A. P. Wilska, Optik (Stuttg.) 26, 247 (1967).
[58] R. Vassoille, C. Guittard, E. Pernoux, and R. Bernard, in ref. 54, v. 1, p. 179.
[59] a) C. Guittard, S. Guittard, and R. Bernard, Bull. Soc. Chim. France, Numero spécial, 3327 (1970); b) L. Laydevant, C. Guittard, and R. Bernard, Proc. of the 5th European Conference on Electron Microscopy, Manchester, 1972, p. 662.
[60] J. R. Garood and W. C. Nixon, in ref. 47, p. 95.
[61] R. E. Ogilvie, M. A. Schipport, S. H. Moll, and D. M. Koffman, Proc. of the 2nd Symposium on Scanning Electron Microscopy, Chicago, IITRI, 1969, p. 425.
[62] J. P. Flemming, J. Sci. Instr., ser. 2, 1, 1179 (1968).
[63] J. E. Cline, J. M. Morris, and S. Schwartz, IEEE Trans. Electron. Dev. ED-16, 371 (1969); D. B. Wittry and P. A. Sullivan, in ref. 54, v. 1, p. 205.
[64] F. Kuhlmann, P. Lieckfeldt, and R. Gradewald, Exper. Techn. Phys. 20, 63 (1972).
[65] W. Schwartze, Optik 25, 260 (1967).
[66] S. Leisegang, Electron Microscopy (Russian translation), Moscow, IL, 1960.
[67] W. Schwartze, Vorträge auf. 9. Tagung Dtsch. Ges. für Electronenmikroskopie, Freiburg, 1959.
[68] W. Schwartze, a) Naturwiss. 52, 448 (1965); b) Exper. Techn. Phys. 11, 92 (1963).
[69] S. Ya. Yavor, Fokusirovka zaryazhennykh chastits kvadrupol'nymi linzami (Focusing of Charged Particles by Quadrupole Lenses), Moscow, Atomizdat, 1968.
[70] A. B. Bok, J. Kramer, and J. B. Le Poole, in ref. 6, Appendix 9.
[71] N. N. Sedov, a) Izv. AN SSSR, ser. fiz. 34, 1529 (1970) [Bull. USSR Acad. Sci., Phys. Ser., p. 1356]; b) J. Micr. 9, 1 (1970).
[72] G. V. Spivak, I. I. Prilezhaeva, and V. K. Azovtsev, Dokl. Akad. Nauk SSSR 100, 965 (1955).
[73] M. E. Barnett and W. C. Nixon, Optik 26, 310 (1967).
[74] A. E. Luk'yanov, G. V. Spivak, N. N. Sedov, and V. I. Petrov, Izv. AN SSSR, ser. fiz. 32, 987 (1968) [Bull. USSR Acad. Sci., Phys. Ser., p. 915].
[75] G. Forst and B. Wende, Z. Angew. Phys. 17, 479 (1964).
[76] a) R. D. Ivanov, Candidate's dissertation, Moscow State University, 1963; b) R. D. Ivanov and M. G. Abalmazova, Prib. Tekh. Éksp., No. 5, 192 (1966) [Instrum. Exp. Tech.].
[77] D. Wiskott, Optik 13, 463, 481 (1956).
[78] J. Heydenreich, a) Exper. Techn. Phys. 10, 346 (1962); b) in ref. 55, p. 233.
[79] U. Brand and W. Schwartze, Exper. Techn. Phys. 11, 18 (1963).
[80] M. E. Barnett and L. England, Optik 27, 341 (1968).
[81] L. Mayer, J. Appl. Phys. 28, 259 (1957).
[82] G. V. Spivak and V. I. Lyubchenko, Izv. AN SSSR, ser. fiz. 23, 697 (1959) [Bull. USSR Acad. Sci., Phys. Ser. p. 691].
[83] G. V. Spivak, R. D. Ivanov, O. P. Pavlyuchenko, and N. N. Sedov, ibid. 27, 1139 (1963) [Bull. USSR Acad. Sci., Phys. Ser., p. 1120].
[84] N. N. Sedov, A. E. Luk'yanov, and G. V. Spivak, ibid. 32, 996 (1968) [Bull. USSR Acad. Sci., Phys. Ser., p. 923].
[85] M. S. Cohen and K. J. Harte, J. Appl. Phys. 40, 3597 (1969).
[86] R. S. Gvozdover, Radiotekh. i élektron. 15, 2653 (1970) [Radio Engineering and Electronic Physics].
[87] N. N. Sedov, Vestn. MGU, ser. III (Fizika Astronomiya 12 (1), 106 (1971) [Moscow University Physics Bulletin 26, 79 (1971)].
[88] N. N. Sedov, Izv. AN SSSR, ser. fiz. 32, 1175 (1968) [Bull. USSR Acad. Sci., p. 1091].
[89] A. N. Tikhonov, Dokl. Akad. Nauk SSSR 151, 501; 153, 49 (1963).
[90] W. Schwartze, in ref. 6, p. 15.
[91] O. M. Artamonov and S. A. Komolov, Radiotekh. i élektron. 11, 2186 (1966) [Radio Engineering and Electronic Physics].
[92] O. M. Aratmonov, N. B. Gerasimova, and S. A. Komolov, Optikomekh. prom. 33 (12), 17 (1966).
[93] M. E. Barnett and W. C. Nixon, in ref. 55, p. 231; Optik 26, 310 (1967).
[94] O. M. Artamonov, Candidate's dissertation, Leningrad State University, 1967.
[95] A. B. Bok, J. B. Poole, and J. Roos, in ref. 47, p. 101.
[96] S. A. Komolov, Candidate's dissertation, Leningrad State University, 1970.
[97] H. Lichte, G. Möllenstedt, and H. Wahl, Zs. Phys. 249, 456 (1972).
[98] A. J. Hermans and J. A. Petterson, J. Eng. Math. (Netherlands) 4, 141 (1970).
[99] E. Soa, Optik 22, 66 (1965).
[100] W. Schwartze, Optik 23, 614 (1965).
[101] R. S. Gvozdover and B. Ya. Zel'dovich, Radiotekh. i élektron. 18 (1973).
[102] A. B. Bok, J. B. Poole, and J. Roos, in ref. 47, p. 103.
[103] a) O. M. Artamonov and S. A. Komolov, Radiotekh. i élektron. 15, 220 (1970) [Radio Engineering and Electronic Physics]; b) Izv. AN SSSR, ser. fiz. 34, 1548 (1970) [Bull. USSR Acad. Sci., Phys. Ser., p. 1373]; c) ibid. 36, 1961 (1972) [Bull. USSR Acad. Sci., Phys. Ser., p. 1734]; d) in ref. 54, 1, p. 193.
[104] O. M. Artamonov, G. N. Brodskiĭ, and S. A. Komolov, Voprosy élektroniki tverdogo tela, Collection 2 (No. 15), Scholarly Publications, Leningrad State University, No. 354 (ser. fiz. nauk), 37 (1968); O. M. Artamonov, S. A. Komolov, L. M. Kulimanina, and N. V. Plitkina, ibid, Collection 3 (No. 16), 75 (1970).
[105] M. V. Nazarov and N. N. Sedov, Izv. AN SSSR, ser. fiz. 36, 2013 (1972) [Bull. USSR Acad. Sci., Phys. Ser., p. 1779].
[106] M. E. Barnett, Appl. Phys. Lett. 12, 229 (1968).
[107] O. I. Szentesi, J. Appl. Phys. 42, 5180 (1971); T. Warminski, in ref. 59(b), p. 28.
[108] O. M. Artamonov, G. G. Dutov, S. A. Komolov, and O. M. Smirnov, Élektronnaya tekhnika, ser. 4 (Élektronnoluchevye i fotoélektricheskie pribory), No. 5, 274 (1968).

[109] L. Mayer, J. Appl. Phys. 28, 975 (1957).
[110] L. Mayer, ibid. 29, 658, 1003, 1454 (1958).
[111] L. Mayer, ibid. 30, 252, 1101 (1959).
[112] L. Mayer, J. Phys. Soc. Japan 17, Suppl. B-1, 547 (1962).
[113] L. Mayer, in ref. 8, JJ-2.
[114] G. V. Spivak, O. P. Pavlyuchenko, and A. E. Luk'yanov, Izv. AN SSSR, ser. fiz. 30, 813 (1966) [Bull. USSR Acad. Sci., Phys. Ser., p. 843].
[115] J. Kranz and H. Bialas, Optik 18, 178 (1961).
[116] G. V. Spivak, R. D. Ivanov, O. P. Pavlyuchenko, N. N. Sedov, and V. F. Shvets, Izv. AN SSSR, ser. fiz. 27, 1210 (1963) [Bull. USSR Acad. Sci., Phys. Ser., p. 1187].
[117] O. P. Pavlyuchenko, Candidate's dissertation, Msocow State University, 1967.
[118] R. S. Gvozdover, Candidate's dissertation, Moscow State University, 1970.
[119] R. S. Gzzozdove and V. I. Petrov, Radiotekh. i élektron. 17, 433 (1972) [Radio Engineering and Electronic Physics].
[120] V. J. Petrov, A. E. Luk'yanov, R. S. Gvozdover and G. V. Spivak, in ref. 54, p. 25.
[121] V. I. Petrov, A. E. Luk'yanov, and G. V. Spivak, Vestn. MGU, ser. III (Fizika Astronomiya) 8 (6), 102 (1967) [Moscow University Physics Bulletin 22, No. 6, 60 (1967)].
[122] N. N. Sedov, G. V. Spivak, V. I. Petrov, A. E. Luk'yanov, and É. I. Rau, Izv. AN SSSR, ser. fiz. 32, 1005 (1968) [Bull. USSR Acad. Sci., Phys. Ser., p. 932].
[123] N. N. Sedov, G. V. Spivak, V. I. Petrov, and A. E. Luk'yanov, Radiotekh. i élektron. 13, 379 (1968) [Radio Engineering and Electronic Physics].
[124] V. I. Petrov, A. E. Luk'yanov, and R. S. Gvozdover, Vestn. MGU, ser. III (Fizika. Astronomiya) 11 (4), 441 (1970) [Moscow University Physics Bulletin 25, No. 4, 60 (1970)].
[125] R. S. Gvozdover, Radiotekh. i élektron. 17, 1697 (1972) [Radio Engineering and Electronic Physics].
[126] G. V. Spivak, R. S. Gvozdover, A. E. Luk'yanov, N. N. Sedov, V. I. Petrov, and A. I. Butylkin, Izv. AN SSSR, ser. fiz. 32, 1211 (1968) [Bull. USSR Acad. Sci., Phys. Ser., p. 1122].
[127] A. E. Luk'yanov, N. N. Sedov, G. V. Spivak, and R. S. Gvosdover, in ref. 47, p. 105.
[128] G. V. Spivak, E. M. Dubinina, V. G. Dyukov, A. E. Luk'yanov, N. N. Sedov, V. I. Petrov, O. P. Pavlyuchenko, G. V. Saparin, and A. N. Nevzorov, Izv. AN SSSR, ser. fiz. 32, 1098 (1968) [Bull. USSR Acad. Sci., p. 1023].
[129] a) É. I. Rau, A. E. Luk'yanov, G. V. Spivak, R. S. Gvozdover, ibid. 34, 1539 (1970) [Bull. USSR Acad. Sci., Phys. Ser., p. 1365]; b) V. N. Gusev, O. M. Kudryavtsev, A. M. Lavrukhin, É. I. Rau, and O. A. Ushakov, ibid. 36, 1327 (1972) [Bull. USSR Acad. Sci., Phys. Ser., p. 1184].
[130] C. W. Bates and L. England, Appl. Phys. Lett. 14, 390 (1969).
[131] G. V. Spivak, I. A. Pryamkova, and V. N. Lepeshinskaya, Dokl. Akad. Nauk SSSR 130, 751 (1960) [Sov. Phys.-Doklady 5, 110 (1960)].
[132] G. V. Spivak, B. B. Schischkin, A. E. Luk'yanov, K. A. Mitschurina, in ref. 6, p. 109; b) S. P. Newberry, J. Appl. Phys. 37, 3931 (1966).
[133] E. Igras, Bull. Ac. Polon. des Sci. (Math., Astr., Phys.) 9, 403 (1961).
[134] E. Igras, Proc. of the Intern. Conference on Physics of Semiconductors, L., 1962, p. 832.
[135] E. Igras, and T. Warminski, Phys. Stat. Sol. 13, 169 (1966); 19, K67; 20, K5 (1967); 27, 69 (1968).
[136] E. Igras and T. Warminski, in ref. 47, p. 109.
[137] E. Igras, W. Przyborski, and T. Warminski, Phys. Stat. Sol. 35, K107 (1969).
[138] a) K. N. Maffitt, J. Vac. Sci. Technol. 2, 285 (1965); b) F. L. English, H. K. Parsons, R. B. Schoolar, and H. R. Riedl, J. Appl. Phys. 40, 3293 (1969).
[139] J. Heydenreich, Heterojunctions and Layer Structure (Intern. Conference on Physics and Chemics of Semiconductors), v. 3, Budapest, 1971, p. 133.
[140] O. I. Szentesi and M. E. Barnett, J. Sci. Instr. E2, 855 (1969).
[141] G. Bartz and G. Weissenberg, Naturwiss. 44, 229 (1957).
[142] N. N. Sedov, G. V. Spivak, and R. D. Ivanov, Izv. AN SSSR, ser. fiz. 26, 1339 (1962) [Bull. USSR Acad. Sci., Phys. Ser.].
[143] A. E. Luk'yanov and L. O. Petrova, Radiotekh. i élektron. 16, 891 (1971) [Radio Engineering and Electronic Physics]; N. N. Sedov, Vestn. MGU, ser. III (Fizika. Astronomiya 12 (5), 609 (1971) [Moscow University Physics Bulletin 26, No. 5, 92 (1971)].
[144] W. Schwartze, Čech. čas. fys. 12, 488 (1962).
[145] G. V. Spivak, A. E. Luk'yanov, and M. G. Abalmazova, Izv. AN SSSR, ser. fiz. 28, 1382 (1964) [Bull. USSR Acad. Sci., Phys. Ser., p. 1287].
[146] F. Lenz and E. Krimmel, Zs. Phys. 175, 235 (1963).
[147] M. G. Abalmazova, N. N. Sedov, and R. D. Ivanov, Izv. AN SSSR, ser. fiz. 34, 1554 (1970) [Bull. USSR Acad. Sci., Phys. Ser., p. 1378].
[148] O. M. Artamonov and C. A. Komolov, see ref. 104, collection 3 (No. 16), 80 (1970).
[149] L. Mayer, J. Appl. Phys. 34, 2088 (1963).
[150] T. Warminski, Phys. Stat. Sol. a3, K159 (1970).
[151] G. V. Spivak and R. D. Ivanov, Izv. AN SSSR, ser. fiz. 27, 1203 (1963) [Bull. USSR Acad. Sci., Phys. Ser., p. 1180].
[152] R. D. Ivanov and M. G. Abalmazova, Zh. Tekh. Fiz. 37, 1351 (1967) [Sov. Phys.-Tech. Phys. 12, 982 (1967).
[153] M. G. Abalmazova, V. P. Demidov, and R. D. Ivanov, Élektronaya tekhnika (Electronic Technology), ser. 6, Mikroélektronika (Microelectronics), No. 1 (22), 69 (1970); V. I. Karasev, A. I. Korobov, and M. G. Abalmazova, Radiotekh. i élektron. 16, 465 (1971) [Radio Engineering and Electronic Physics].
[154] T. Warminski and I. Glass, Phys. Stat. Sol. a8, K17 (1971).
[155] G. V. Spivak and A. E. Luk'yanov, Izv. AN SSSR, ser. fiz. 30, 781 (1966) [Bull. USSR Acad. Sci., Phys. Ser., p. 809]; A. E. Luk'yanov and G. V. Spivak, see ref. 55, p. 611.
[156] R. S. Gvozdover, I. V. Karpova, S. G. Kalashnikov, A. E. Luk'yanov, É. I. Rau, and G. V. Spivak, Radiotekh. i élektron. 15, 2368 (1970) [Radio Engineering and Electronic Physics]; R. S. Gvozdover, J. V. Karpova, S. G. Kalashnikov, A. E. Luk'yanov, E. I. Rau, and G. V. Spivak, Phys. Stat. Sol. a5, 65 (1971).
[157] O. I. Szentesi and E. A. Ash, IEEE Trans. Sonics and Ultrasonics SU-17, 66 (1970); O. I. Szentesi, J. Phys. E5, 563 (1972).
[158] C. Guittard, These Doct. Sci. Phys. (Fac. Sci. Univ. Lyon, 1966); C. Guittard, J. P. Briffaut, R. Bernard, and E. Pernoux, C. R. Acad. Sci. 259, 371 (1964); C. Guittard and E. Pernoux, ibid. 261, 5358 (1965).
[159] C. Guittard et al., ibid. B264, 592 (1967); see ref. 47, p. 107.

[160] M. Babout, L. Laydevant, and C. Guittard, see ref. 54, v. 1, p. 271.
[161] C. Guittard and R. Bernard, see ref. 54, p. 275.
[162] C. Guittard et al., J. Micr. **5**, 13a (1966); 6, 18a (1967).
[163] G. V. Spivak, A. E. Luk'yanov, S. D. Toshev, and V. A. Koptsik, Izv. AN SSSR, ser. fiz. **27**, 1199 (1963) [Bull. USSR Acad. Sci., Phys. Ser., p. 1177].
[164] F. L. English, J. Appl. Phys. **39**, 128, 2302 (1968).
[165] T. Someya and J. Kobayashi, Proc. of 28th Annual Meeting of the Electron Microscopy Society of America (Houston, Tex., USA, October 1970), Baton Rouge, La., USA, Claitors Publ. Division 1970, p. 478.
[166] J. Kobayashi, T. Someya, and Y. Furuhata, Phys. Lett. **A38**, 309 (1972); K. N. Maffitt, J. Appl. Phys. **39**, 3878 (1968).
[167] T. Someya and J. Kobayashi, Phys. Stat. Sol. **4**, K161 (1971).
[168] T. Someya and J. Kobayashi, see ref. 54, p. 627.
[169] T. Someya et al., J. Phys. Soc. Japan **28**, 374 (1970).
[170] G. Koch, Jeanaer Jahrbuch **11**, 179 (1958); Acustica **10**, 167 (1960).
[171] R. S. Gvozdover, A. E. Luk'yanov, G. V. Spivak, V. E. Lyamov, É. I. Rau, and A. I. Butylkin, Radiotekh. i élektron. **13**, 2276 (1968) [Radio Engineering and Electronic Physics].
[172] R. S. Gvozdover, A. E. Luk'yanov, G. V. Spivak, É. I. Rau, and M. V. Bykov, Izv. AN SSSR, ser. fiz. **34**, 1483 (1970) [Bull. USSR Acad. Sci., Phys. Ser., p. 1318].
[173] R. S. Gvozdover, A. E. Luk'yanov, G. V. Spivak, and E. I. Rau, see ref. 54, v. 1, p. 193.
[174] R. S. Gvozdover, see ref. 59b, p. 504.
[175] M. C. Antoshin, G. V. Spivak, A. E. Luk'yanov, E. I. Rau, O. A. Ushakov, A. I. Akishin, and G. A. Tokarev, see ref. 59b, p. 506; G. V. Spivak, M. K. Antoshin, A. E. Luk'yanov, É. I. Rau, and I. Bartel', Izv. AN SSSR, ser. fiz. **36**, 1954 (1972) [Bull. USSR Acad. Sci., Phys. Ser., p. 1727].
[176] G. C. McLeod and R. M. Oman, J. Appl. Phys. **39**, 2756 (1968).
[177] R. D. Ivanov and M. G. Abalmazova, Radiotekh. i élektron. **16**, 447 (1971) [Radio Engineering and Electronic Physics]; J. Heydenreich, see ref. 59b, p. 490.
[178] G. V. Spivak and I. A. Pryamkova, in "Magnitnaya struktura ferromagnetikov" (Magnetic Structure of Ferromagnets), ed. L. V. Kirenskii, Novosibirsk, Siberian Div., AN SSSR, 1960, p. 185; J. D. Kuehler, IBM, J. Res. and Develop. **4**, 202 (1960); G. V. Spivak, L. V. Kirenskiĭ, R. D. Ivanov, and N. N. Sedov, Izv. AN SSSR, ser. fiz. **25**, 1465 (1961) [Bull. USSR Acad. Sci., Phys. Ser.]; K. N. Maffitt, D. S. Lo, A. L. Olson, and E. J. Torok, Rev. Sci. Instr. **39**, 259 (1968).
[179] G. V. Spivak, O. P. Pavljutschenko, R. D. Ivanov, and G. P. Netischenskaja, see ref. 6, p. 293.
[180] R. D. Ivanov, Zh. Tekh. Fiz. **35**, 145 (1965) [Sov. Phys.-Tech. Phys. **10**, 110 (1965)].
[181] G. V. Spivak and A. E. Luk'yanov, Izv. AN SSSR, ser. fiz. **30**, 803 (1966) [Bull. USSR Acad. Sci., Phys. Ser., p. 831].
[182] G. V. Spivak, A. E. Luk'yanov, E. I. Rau, and R. S. Gvozdover, Intermag-71, IEEE Trans. Magnet. **MAG-7**, 684 (1971).
[183] C. Guittard et al., C. R. Acad. Sci. **B264**, 924 (1967).
[184] G. Weissenberg, Patent FRG No. 974698 (1961).
[185] O. Bostanjoglo and G. Seigel, Cryogenics **7** (3), 157 (1967).
[186] S. T. Wang et al., Trudy X Mezhdunarodnoĭ konferentsii po fizike nizkikh temperatur (Proceedings, X Internat. Conf. on Low-Temp. Phys.), Moscow, 1966, **2A**, Moscow, VINITI, 1967, p. 364.
[187] V. I. Petrov, G. V. Spivak, and O. P. Pavlyuchenko, Usp. Fiz. Nauk **102**, 529 (1970) [Sov. Phys.-Uspekhi **13**, 766 (1971)].

Translated by C. S. Robinson